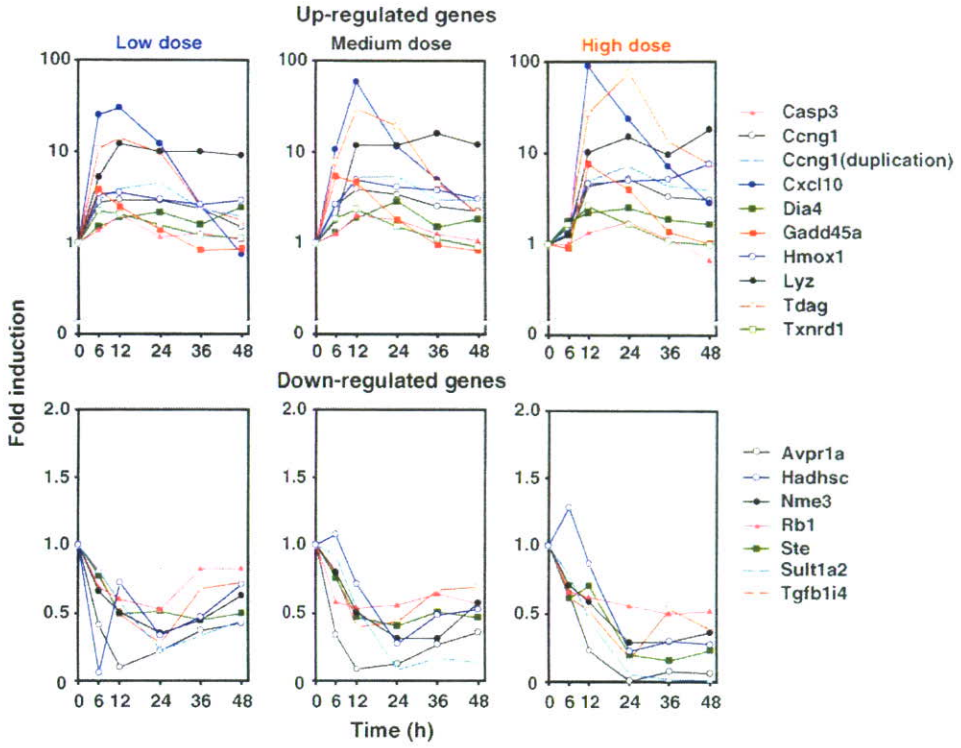

Fig. 5. Gene expression profiles of the selected genes. The up-regulated group consisted of nine genes and the down-regulated group seven genes. Total RNA samples from four rats were pooled and used for this analysis. Symbols, accession numbers and gene names are as follows: Casp3, NM_012922, caspase 3, apoptosis related cysteine protease (ICE-like cysteine protease) mRNA; Ccng1, NM_012923, cyclin G1 mRNA; Cxcl10, U22520, interferon inducible protein 10 (IP-10) mRNA, complete cds; Dia4, NM_017000, diaphorase (NADH/NADPH) mRNA; Gadd45a, NM_024127, growth arrest and DNA-damage-inducible 45 alpha mRNA; Hmox1, NM_012580, heme oxygenase (decycling) 1 mRNA; Lyz, NM_012771, lysozyme mRNA; Tdag, NM_017180, T-cell death associated gene mRNA; Txnrd1, NM_031614, thioredoxin reductase 1 mRNA; Avpr1a, Z11690, mRNA for V1a arginine vasopressin receptor; Hadhsc, NM_057186, L-3-hydroxyacyl-coenzyme A dehydrogenase, short chain mRNA; Nme3, NM_053507, expressed in non-metastatic cells 3, protein (nucleoside diphosphate kinase) mRNA; Rb1, D25233, mRNA for retinoblastoma protein, partial sequence; Ste, NM_012883, sulfotransferase, estrogen preferring mRNA; Sult1a2, NM_031732, sulfotransferase family 1A, member 2 mRNA; Tgfb1i4, NM_013043, transforming growth factor beta 1-induced transcript 4 mRNA.

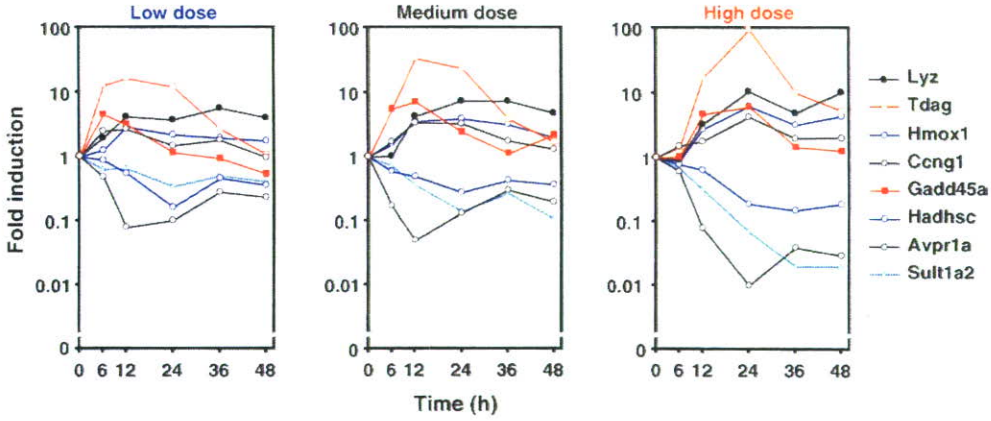

Fig. 6. Real-time RT-PCR analysis of the expression of the representative genes. Total RNA samples from four rats were pooled and used for real-time RT-PCR analysis. This figure shows the representative five up-regulated and three down-regulated genes as shown in Fig. 5. Official gene names are described in Fig. 5.

order to confirm the gene expression changes found in the DNA microarray analysis, real-time RT-PCR analysis was performed in eight representative genes (Fig. 6). The expression profiles and extent of these eight gene expressions were almost the same as those of the DNA microarray.

4. Discussion

Gene expression changes have been used to provide specific mechanistic information concerning the mode of action of toxicants. Toxicogenomics is an approach that applies microarray technology to toxicological evaluation paradigms. Toxicogenomic gene expression studies have been facilitated by the recent development of high-density microarrays.

In our previous study [16], the relationship between the hepatic gene expression profiles and hepatotoxicity was investigated in rats using in five typical hepatotoxicants. The mRNA of TA (400 mg/kg weight) administered rats was analyzed. Finally, 17 possible potential hepatotoxicity markers were proposed. In the present study, in order to evaluate the gene expression for hepatotoxicity in detail, we evaluated the effects of three dosages of TA, which causes zone-3 necrosis [17], by using a 9936 gene-spotted microarray slide. The dosage was selected according to a previous report [17]. The high-, medium-, low-dose administration was expected to cause severe toxicity, low toxicity and no toxicity, respectively. In this study, we compared between the extent of toxicity and the changes of gene expression in detail.

Previously, the effects of 300, 400 or 500 mg/kg weight of TA-administration in rats were reported [5,11,16]. The maximal point of TA toxicity estimated from the serum AST and ALT activities was 24 h after the administration. The present results were the same as those of previous reports. In the present study, the unconjugated bilirubin was not increased by TA-administration but the conjugated bilirubin was increased at 24 h by the high dosage of TA. These data confirmed that the toxicity model of TA-administration was successfully conducted in the present study. Additionally, the toxic time points of each dosage were estimated as 24 h.

Hierarchical clustering was performed to examine the gene expression data derived from the microarray analysis. All groups were extensively sorted into the early phase (6 and 12 h) or in the late phase (24, 36 and 48 h). In the early phase, the clusters were sorted in a time-dependent manner. Previously, Bulera et al. [18], reported in a comparison between low dose (40 mg/kg) and high dose (500 mg/kg) at early times (low dose: 3 and 6 h; high dose: 8 h) after the administration in rats using a microarray method, reported that all three groups were sorted into a the similar cluster. This result was similar to that of early phase in the present experiment (Fig. 2A). On the other hand, the late phase cluster was clustered in a dose-dependent manner (Fig. 2A). Therefore, we report here that the hierarchical clustering analysis demonstrated that the gene expression patterns were changed dose independently in the early phase of hepatotoxicity, but in dose dependently in the late phase of hepatotoxicity. Furthermore, hierarchical clustering at different dosages showed the same result as shown in Fig. 2B. The hierarchical distance between the early and the late phase were separated in a dose-dependent manner as shown by the dendrograms (Fig. 2B), suggesting that there was a certain relationship between the extent of hepatotoxicity and the gene expression pattern.

QT clustering based on the time after TA-administration was performed. This method can estimate the majority of gene expression profiles as previously reported [16]. As shown in Fig. 3, this result confirmed our finding from the hierarchical clustering analysis. Moreover, the hierarchical clustering and QT clustering based on the time after TA-administration also suggest that there was a dose dependency in the extent of the gene expression changes after the hepatotoxicity appeared.

QT clustering based on the TA dosage was also performed (Fig. 4). The profiles of both the average and median values from the QT clustering reflected the changes in biochemical markers. This result confirmed those of our previous study [16]. Furthermore, the present study indicated that the changes of the gene expression in the QT clustering became distinct in a dose-dependent manner. Taking these results into consideration, in this study, we demonstrated that the hepatic gene expression profiles are independent of the TA dosage and reflect the changes in the serum biochemical markers.

Category classification of the genes affected by TA-administration showed that the numbers of down-regulated genes were greater than those of the up-regulated genes, as reported previously [16].

Bulera et al. [18] reported the gene expression data after 24 h of TA-administration (500 mg/kg). In their study, expression changes were analyzed in 1600 genes and they showed that 133 genes were up-regulated and 163 genes were down-regulated. The microarray slides used in the present study spotted 49 of their 133 up-regulated genes (36.8%) and 68 of their 163 down-regulated genes (41.7%). In total, 117 of the 296 genes (39.5%) were spotted. In the present study, 39 of the 49 genes (79.6%) were up-regulated and 64 of the 68 genes (94.1%) were down-regulated (data not shown).

For example, FMO1, which metabolizes TA to a toxic metabolite, was down-regulated (<0.1-fold). In a total of 103 of 117 genes (88.0%), the expressions were similar to those reported by Bulera et al. [18].

In the previous study, using five traditional hepatotoxicants including TA we performed simultaneous measurements using other microarray slides (Rat Drug Response Chip, Hitachi) [16]. Most of the genes showed similar expression profiles to those of the present study. The expression profiles were confirmed in eight representative genes by real-time RT-PCR, which showed almost the same profile as that of the DNA microarray. This result suggested that our candidate genes could be sensitive markers for hepatotoxicity. However, the relationship between these genes was not clarified.

In summary, the present study demonstrated that there are distinct gene expression differences between pretoxic- and toxic-periods (Fig. 2), there is a dose dependency in the extent of the major gene expression changes after toxicity appears (Fig. 3), the major gene expression profiles reflect the biochemical marker activities (Fig. 4), and the candidate genes identified in our previous microarray analysis could be used as sensitive markers for hepatotoxicity (Fig. 5). In conclusion, the potential toxic effects appearing as gene expression changes are independent of the dosage of TA. The major gene expression profiles estimated by QT clustering analysis would be a sensitive marker for predicting potential hepatotoxicity.

Acknowledgements

This work was supported in part by a grant from the Ministry of Education, Science, Sports, and Culture of Japan, and by Research on Advanced Medical Technology, Health and Labor Science Research Grants from the Ministry of Health, Labor and Welfare of Japan. We thank Mr. Brent Bell for reviewing the manuscript.

References

[1] M. Bittner, P. Meltzer, J. Trent, Data analysis and integration: of steps and arrows, Nat. Genet. 22 (1999) 213–215.
[2] S. Tavazoie, J.D. Hughes, M.J. Campbell, R.J. Cho, G.M. Church, Systematic determination of genetic network architecture, Nat. Genet. 22 (1999) 281–285.
[3] L.J. Heyer, S. Kruglyak, S. Yooseph, Exploring expression data: identification and analysis of coexpressed genes, Genome Res. 11 (1999) 1106–1115.
[4] A.L. Hunter, M.A. Holscher, R.A. Neal, Thioacetamide-induced hepatic necrosis. I. Involvement of the mixed-function oxidase enzyme system, J. Pharmacol. Exp. Ther. 200 (1977) 439–448.
[5] T. Wang, K. Shankar, M.J. Ronis, H.M. Mehendale, Potentiation of thioacetamide liver injury in diabetic rats is due to induced CYP2E1, J. Pharmacol. Exp. Ther. 294 (2000) 473–479.
[6] M.C. Dyroff, R.A. Neal, Identification of the major protein adduct formed in rat liver after thioacetamide administration, Cancer Res. 41 (1981) 3430–3435.
[7] W.R. Porter, R.A. Neal, Metabolism of thioacetamide and thioacetamide *S*-oxide by rat liver microsomes, Drug Metab. Dispos. 6 (1978) 379–388.
[8] W.R. Porter, M.J. Gudzinowicz, R.A. Neal, Thioacetamide-induced hepatic necrosis. II. Pharmacokinetics of thioacetamide and thioacetamide *S*-oxide in the rat, J. Pharmacol. Exp. Ther. 208 (1979) 386–391.
[9] N. Sanz, C. Diez-Fernandez, A.M. Alvarez, L. Fernandez-Simon, M. Cascales, Age-related changes on parameters of experimentally induced liver injury and regeneration, Toxicol. Appl. Pharmacol. 154 (1999) 40–49.
[10] N. Sanz, C. Diez-Fernandez, D. Andres, M. Cascales, Hepatotoxicity and aging: endogenous antioxidant systems in hepatocytes from 2-, 6-, 12-, 18- and 30-month-old rats following a necrogenic dose of thioacetamide, Biochim. Biophys Acta 1587 (2002) 12–20.
[11] A. Zaragoza, D. Andres, D. Sarrion, M. Cascales, Potentiation of thioacetamide hepatotoxicity by phenobarbital pretreatment in rats. Inducibility of FAD monooxygenase system and age effect, Chem. Biol. Interact. 124 (2000) 87–101.
[12] A. Gozdz, E. Szczepanska-Sadowska, K. Szczepanska, W. Maslinski, B. Luszczyk, Vasopressin V1a, V1b and V2 receptors mRNA in the kidney and heart of the renin transgenic TGR(mRen2)27 and Sprague–Dawley rats, J. Physiol. Pharmacol. 53 (2002) 349–357.
[13] R.S. Ge, M.P. Hardy, Decreased cyclin A2 and increased cyclin G1 levels coincide with loss of proliferative capacity in rat Leydig cells during pubertal development, Endocrinology 138 (1997) 3719–3726.
[14] S.A. Shain, Exogenous fibroblast growth factors maintain viability, promote proliferation, and suppress GADD45alpha and GAS6 transcript content of prostate cancer cells genetically modified to lack endogenous FGF-2, Mol. Cancer Res. 2 (2004) 653–661.
[15] J.M. Rodriguez Parkitna, W. Bilecki, P. Mierzejewski, R. Stefanski, A. Ligeza, A. Bargiela, B. Ziolkowska, W. Kostowski, R. Przewlocki, Effects of morphine on gene expression in the rat amygdala, J. Neurochem. 91 (2004) 38–48.
[16] K. Minami, T. Saito, M. Narahara, H. Tomita, H. Kato, H. Sugiyama, M. Katoh, M. Nakajima, T. Yokoi, Relationship between hepatic gene expression profiles and hepatotoxicity in five typical hepatotoxicant-administered rats, Toxicol. Sci. 87 (2005) 296–305.
[17] H.J. Zimmerman, Hepatotoxicity: The Adverse Effects of Drugs and Other Chemicals on the Liver, 2nd ed., Lippncott Williams & Wilkins, Philadelphia, 1999, pp. 266–267.
[18] S.J. Bulera, S.M. Eddy, E. Ferguson, T.A. Jatkoe, J.F. Reindel, M.R. Bleavins, F.A. De La Iglesia, RNA expression in the early characterization of hepatotoxicants in Wistar rats by high-density DNA microarrays, Hepatology 33 (2001) 1239–1258.

J. Biochem. 139, 527–534 (2006)
doi:10.1093/jb/mvj055

Binding of Steroidogenic Factor-1 to the Regulatory Region Might Not Be Critical for Transcriptional Regulation of the Human *CYP1B1* Gene

Yuki Tsuchiya[1], Miki Nakajima[1], Shingo Takagi[1], Miki Katoh[1], Wenchao Zheng[2], Colin R Jefcoate[2] and Tsuyoshi Yokoi[1,*]

[1]Drug Metabolism and Toxicology, Division of Pharmaceutical Sciences, Graduate School of Medical Science, Kanazawa University, Kakuma-machi, Kanazawa 920-1192; and [2]Department of Pharmacology, Medical Science Center, University of Wisconsin, 1300 University Avenue, Madison, WI 53706, USA

Received November 18, 2005; accepted January 10, 2006

Cytochrome P450 (CYP) 1B1, which catalyzes 17β-estradiol 4-hydroxylation, is expressed in steroid-related tissues including ovary, testis, and adrenal gland. Generally, the expressions of steroidogenic CYPs are transcriptionally regulated by steroidogenic factor-1 (SF-1) and cAMP response element (CRE) binding protein (CREB). In the present study, we examined the possibility that the human *CYP1B1* gene might be regulated by SF-1 and CREB. Gel shift analyses revealed that *in vitro* translated SF-1 can bind to the putative SF-1 binding sites, SF-1a (at −1722) and SF-1b (at −2474), on the *CYP1B1* gene. *In vitro* translated CREB barely binds to the putative SF-1 binding sites. Luciferase analysis revealed that a reporter plasmid, pGL3 (−2623/+25), containing the SF-1a and SF-1b elements is transactivated by the concomitant co-expression of SF-1 and protein kinase A (PKA). However, the transcriptional activity is induced by PKA alone. Mutations in the SF-1a and SF-1b elements did not affect the luciferase activity. Thus, the binding of SF-1 to the putative SF-1 binding sites of the human *CYP1B1* gene might not be essential for transcriptional regulation. Interestingly, deletion and mutation analyses indicated that the PKA signaling pathway is involved in the xenobiotic responsive element (XRE)–mediated transactivation of the human *CYP1B1* gene.

Key words: CREB, CYP1B1, gene regulation, PKA; SF-1.

Abbreviations: AhR, aryl hydrocarbon receptor; ARNT, AhR nuclear translocator; CRE, cAMP response element; CREB, CRE binding protein; CYP, cytochrome P450; PKA, protein kinase A; SF-1, steroidogenic factor-1; TCDD, 2,3,7,8-tetrachlorodibenzo-*p*-dioxin; XRE, xenobiotic responsive element.

Cytochrome P450 (CYP)s comprise a multigene family of constitutive and inducible enzymes involved in the oxidative metabolic activation and detoxification of many endogenous and exogenous compounds (*1*, *2*). Human CYP1B1 is mainly expressed in lung, kidney, ovary, uterus, breast, prostate, and adrenal gland (*3*, *4*). Its function involves not only the metabolic activation of a variety of procarcinogens and promutagens, including polycyclic aromatic hydrocarbons (PAHs) and aryl amines (*4*), but also the hydroxylation of the endogenous substrate 17β-estradiol in human (*5*, *6*).

In rat, CYP1B1 expression has been reported to be increased by adrenocorticotropic hormone (ACTH) and cAMP (*7*, *8*). In addition, Zheng *et al.* (*9*, *10*) recently reported that the transcriptional regulation of the rat *CYP1B1* gene is mediated by steroidogenic factor-1 (SF-1) and cAMP response element binding protein (CREB). SF-1 is a member of the orphan nuclear receptor family. SF-1 is expressed in adrenal cortex, testis, ovary, pituitary gonadotrope cells, and hypothalamus (*11*, *12*), and is essential for adrenal development and sexual differentiation (*13*, *14*). SF-1 is activated by the cAMP-dependent protein kinase A (PKA) and plays an important role in regulating the expression of various steroidogenic genes, such as steroidogenic acute regulatory protein (*15*), CYP11A1 (*16*), CYP11B1 (*17*), CYP17 (*18*), and CYP19 (*19*). In the 5′-flanking region of these target genes, SF-1 binds to a consensus sequence (PuPuAGGTCA or PyCAAGGPyPy) as a monomer and enhances the transcriptional activation (*20*).

CREB is a member of the leucine zipper family, which is also activated by the PKA signaling pathway, and recognizes the cAMP response element (CRE) core sequence (TGACGTCA) of the target gene (*21*). SF-1 is involved in cAMP-regulated gene expression, since SF-1 interacts with CREB mediated by the PKA pathway (*22*, *23*).

In the rat *CYP1B1* gene, four SF-1 binding sites and two potential CREs have been identified at −5298 to −5110 (Far Upstream Enhancer Region, FUER) (*9*, *10*). Although the corresponding FUER rat homolog does not exist in the human *CYP1B1* gene, we found two putative SF-1 binding sites at −1722 and −2474 in the human *CYP1B1* gene. This prompted us to investigate the possibility that human CYP1B1 expressed in steroidogenic tissues might also be controlled by SF-1 and CREB. In the present study, we examined the binding of SF-1 or CREB to the putative SF-1 binding sites on the 5′-flanking region of the human *CYP1B1* gene by gel shift analyses. In addition,

*To whom all correspondence should be addressed. Tel/Fax: +81-76-234-4407, E-mail: TYOKOI@kenroku.kanazawa-u.ac.jp

luciferase analyses were performed using various reporter constructs containing the 5′-flanking region of the human *CYP1B1* gene to investigate the involvement of these factors in the transcriptional regulation.

MATERIALS AND METHODS

Chemicals and Reagents—The pGL3-basic plasmid and luciferase reporter assay system were from Promega (Madison, WI). The pCMV-CREB and pCMV-PKA plasmids, which contain the full-length cDNA of human CREB and the catalytic subunit of human PKA, respectively, were purchased from BD Biosciences Clontech (Palo Alto, CA). The pRc/RSV-SF-1 plasmid containing bovine SF-1 cDNA and rabbit anti–bovine SF-1 antiserum were kindly provided by Dr. Ken-Ichirou Morohashi (National Institute of Basic Biology, Okazaki, Japan). [γ-^{32}P]ATP was from Amersham (Buckinghamshire, UK). All primers and oligonucleotides were commercially synthesized by Hokkaido System Sciences (Sapporo, Japan). The mouse anti–human CREB monoclonal antibody was from Santa Cruz Biotechnology (Santa Cruz, CA). All other chemicals and solvents were of the highest grade commercially available.

In Vitro Transcription/translation and Gel Shift Analyses—One microgram of the pTNT-SF-1 plasmid and pTNT-CREB plasmid were incubated at 30°C for 90 min with the T7 TNT quick-coupled transcription/translation system (Promega) in the presence of methionine. The *in vitro* synthesized products were then subjected to gel shift analyses. Synthetic oligonucleotides were labeled with [γ-^{32}P]ATP using T4 polynucleotide kinase (Toyobo, Osaka, Japan). The oligonucleotide sequences are shown in Table 1. The sequence of the consensus SF-1 binding site (cSF) was from the bovine *CYP11B1* gene (*20*) and the sequence of the consensus cAMP response element (CRE) was provided by Santa Cruz Biotechnology. The reaction mixture contained 1 μl of the *in vitro* translated product, 2 μg of poly [dI-dC], 1 μg of salmon sperm DNA, and 30 fmol of radiolabeled probe (~20,000 cpm) with binding buffer [25 mM Hepes-KOH (pH 7.9), 0.5 mM EDTA, 50 mM KCl, 10% glycerol, 0.5 mM dithiothreitol, 0.5 mM (*p*-amidinophenyl) methanesulfonyl fluoride] in a final volume of 15 μl. The binding reaction was performed at 25°C for 30 min. To determine the specificity of the binding to the oligonucleotides, competition experiments were conducted by co-incubation with excess amounts of unlabeled competitors. For super-shift analyses, rabbit anti–bovine SF-1 antiserum or anti–human CREB monoclonal antibody were pre-incubated with the *in vitro* translated product on ice for 15 min, and then each radiolabeled probe was added. DNA-protein complexes were separated under nondenaturing conditions in 4% polyacrylamide gels with 0.5× TBE as the running buffer. The gels were dried, and then the DNA-protein complexes were detected and quantified with a Fuji Bio-Imaging Analyzer BAS 1000 (Fuji Film, Tokyo, Japan).

Plasmid Constructs—The pTNT-SF-1 plasmid was constructed by cloning the full-length bovine SF-1 cDNA digested with *Sac*II and *Xba*I from the pRc/RSV-SF-1 plasmid into the *Xho*I and *Xba*I-digested pTNT vector (Promega). The pTNT-CREB plasmid was constructed by cloning the full-length human CREB cDNA digested with *Eco*RI and *Mlu*I from the pCMV-CREB into the *Eco*RI and *Mlu*I-digested pTNT vector. A series of pGL3-basic plasmids containing the 5′-flanking region of the human *CYP1B1* gene (–2299/+25, –1652/+25, –1022/+25, –910/+25, and –732/+25) and mutated plasmids (–910/XRE3 mt, –910/XRE2 mt, and –910/Sp1-like mt) were constructed in our previous study (*24*). A plasmid containing the 5′-flanking region of the human *CYP1B1* from –2623 to +25 was constructed as follows: a DNA fragment containing the sequence from –2623 to –869 was amplified by PCR using the forward primer adapted to include a *Mlu*I site at the 5′ end, 5′-CGC GTA TCT AAG TTC CCC ATC ATG-3′, and the reverse primer, 5′-GAA AGT CGG CTC CAG TCA TAT CC-3′. After digestion with *Eco*RI, the PCR product was cloned into the *Mlu*I and *Eco*RI-digested pGL3-basic (–2299/+25) plasmid. The orientation of the construct was verified by restriction enzyme digestion or the nucleotide sequence was confirmed by DNA sequencing analysis. Mutated plasmids (–2623/SF-1a mt, –2623/SF-1b mt, and –2623/SF-1a/b mt) were constructed by site-directed mutagenesis with a QuikChange® site-directed mutagenesis kit (Stratagene, La Jolla, CA). For the –2623/SF-1a mt construct, the forward and reverse mutagenic primers were 5′-GGT CTC GAA CTC CTG AAA TCA AGT GAT CCG CCC GC-3′ and 5′-GCG GGC GGA TCA CTT GAT TTC AGG AGT TCG AGA CC-3′, respectively (mutated sites are underlined). For the –2623/SF-1b mt construct, the forward and reverse mutagenic primers were 5′-GGT GGA TCA CCT GAA ATC AGG AGT TTG AGA CCA GCC-3′ and 5′-GGC TGG TCT CAA ACT CCT GAT TTC AGG TGA TCC ACC-3′, respectively. Nucleotide sequences were confirmed by DNA sequencing analysis. The p0.2 plasmid containing the 0.2 kb proximal promoter region of the rat *CYP1B1* gene and the pFUER/0.2 plasmid containing the far upstream enhancer region (FUER) from –5298 to –5188 of the rat *CYP1B1* gene in addition to the 0.2 kb proximal promoter region were previously constructed (*9*).

Cells Culture and Luciferase Assay—The human ovarian granulosa–like tumor cell line KGN (*25*) and the mouse adrenal tumor cell line Y-1 were obtained from Riken Gene Bank (Tsukuba, Japan) and American Type Culture Collection (Rockville, MD), respectively. KGN cells were cultured in a 1:1 mixture of Dulbecco's modified Eagle's medium (DMEM) and Ham's F-12 medium (Nissui Pharmaceutical, Tokyo, Japan) supplemented with 10% (v/v) fetal bovine serum (FBS) (Invitrogen). Y-1 cells were cultured in DMEM supplemented with 10% FBS. These cells were maintained at 37°C under an atmosphere of 5% CO_2–95% air. For the luciferase assays, cells were seeded into 24-well plates (8×10^4 cells/well) and incubated for 24 h before transfection. KGN cells were transfected with 400 ng of *CYP1B1/luc* reporter gene plasmid and 50 ng of pRc/RSV-SF-1 plasmid or pRc/RSV vector in the presence of 50 ng of pCMV-PKA plasmid or pCMV vector using Superfect Transfect Regents (QIAGEN, Hilden, Germany) at a reagent:DNA ratio of 3:1 in 200 μl of serum-free culture medium. After incubation at 37°C for 3 h under an atmosphere of 5% CO_2–95% air, growth medium was added to the cells. Y-1 cells were transfected with the same plasmids as above using Tfx-20 reagent (Promega) at a reagent:DNA ratio of 2.5:1 in 200 μl of

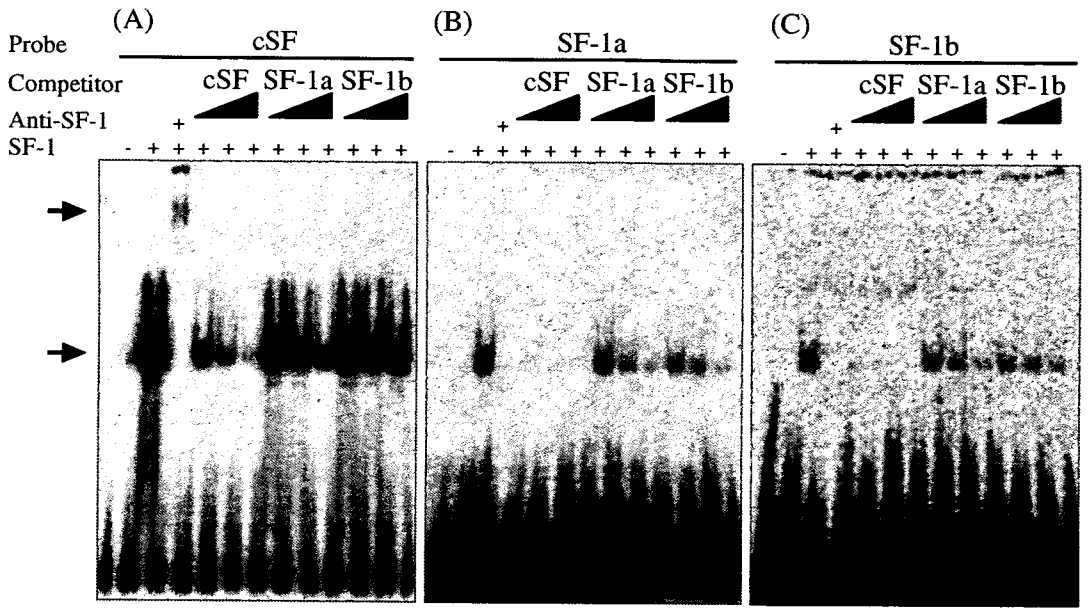

Fig. 1. **Gel shift analyses of the putative SF-1 binding sites on the human *CYP1B1* gene with SF-1.** Radiolabeled cSF (A), SF-1a (B), and SF-1b (C) were used as probes and each cold oligonucleotide was used as a competitor at 200-, 500-, and 1,000-fold molar excesses. For super-shift analyses, rabbit anti–bovine SF-1 serum was pre-incubated with *in vitro* translated SF-1 protein on ice for 15 min, and then the radiolabeled probe was added. DNA-protein complexes were separated under nondenaturing conditions in 4% polyacrylamide gels. The lower arrow indicates the position of the SF-1–dependent shifted band and the upper arrow indicates the super-shifted SF-1 complex.

serum-free culture medium. After incubation at 37°C for 1 h under an atmosphere of 5% CO_2–95% air, growth medium was added to the cells. After 48 h, the cells were resuspended in passive lysis buffer, and then the luciferase activity was measured with a luminometer (WALLAC, Turku, Finland) using a luciferase reporter assay system (Promega). Protein concentrations were determined using the Bradford protein assay regent (Bio-Rad, Hercules, CA) with bovine γ-globulin as the standard. The luciferase activity was normalized to the protein content.

Statistical Analyses—Data are expressed as mean ± SD of triplicate determinations. Statistical significance was determined by analysis of variance and Scheffe's test. A value of $P < 0.05$ was considered statistically significant.

RESULTS

Binding of SF-1 to the Putative SF-1 Binding Sites on the Human CYP1B1 Gene—A computer-assisted homology search revealed two putative SF-1 binding sites, SF-1a at –1722 and SF-1b at –2474, in the 5′-flanking region of the human *CYP1B1* gene. The SF-1a and SF-1b sequences are different from the consensus SF-1 binding sequence (PuPuAGGTCA) in one base. To determine whether SF-1 can bind to the SF-1a or SF-1b sequence on the human *CYP1B1* gene, gel shift analyses were performed (Fig. 1). Oligonucleotides used for the gel shift analyses are shown in Table 1. Using an oligonucleotide containing the consensus SF-1 binding sequence (cSF) as a probe, we confirmed that the *in vitro* translated SF-1 binds to cSF (Fig. 1A). A super-shifted band was observed with anti–SF-1 antiserum. However, the super-shifted band was not observed with normal rabbit IgG (data not shown). The band density was decreased by a cold cSF competitor. In contrast, the competition with the cold competitors of SF-1a and SF-1b was weak. Using SF-1a or SF-1b as a probe, the shifted band was also observed with SF-1, although the intensity was weak (Fig. 1, B and C). The shifted bands were abolished with anti–SF-1 antiserum, and excessive cold cSF competitors robustly diminished the DNA-protein complexes for SF-1a and SF-1b. In contrast, the competition with cold competitors of SF-1a and SF-1b was weak. These results indicate that SF-1 binds to the putative SF-1 binding sites on the human *CYP1B1* gene.

Table 1. **Oligoprobes used for gel shift analyses.**

Probe	Sequence	Position
SF-1a	5′-CGAACTCCTGACCTCAAGTGA-TCCGCCCGC-3′	–1737/–1708
SF-1b	5′-GTGGATCACCTGAGGTCAGGA-GTTTGAGAC-3′	–2491/–2462
cSF	5′-ACATACCCAAGGTCCCCTTT-3′	–337/–318
cCRE	5′-AGAGATTGCCTGACGTCAGA-GAGCTAG-3′	Artificial

Sequence and position of SF-1 binding sites in the human *CYP1B1* gene are listed. Each core region is underlined. SF-1a is actually the reverse complement of the SF-1 binding site. The consensus SF-1 binding site (cSF) sequence is that of the bovine *CYP11B1* gene. The consensus CRE (cCRE) sequence was created by Santa Cruz Biotechnology.

Binding of CREB to the Putative SF-1 Binding Sites on the Human CYP1B1 Gene—The sequences of SF-1a and SF-1b resemble that of the cAMP response element

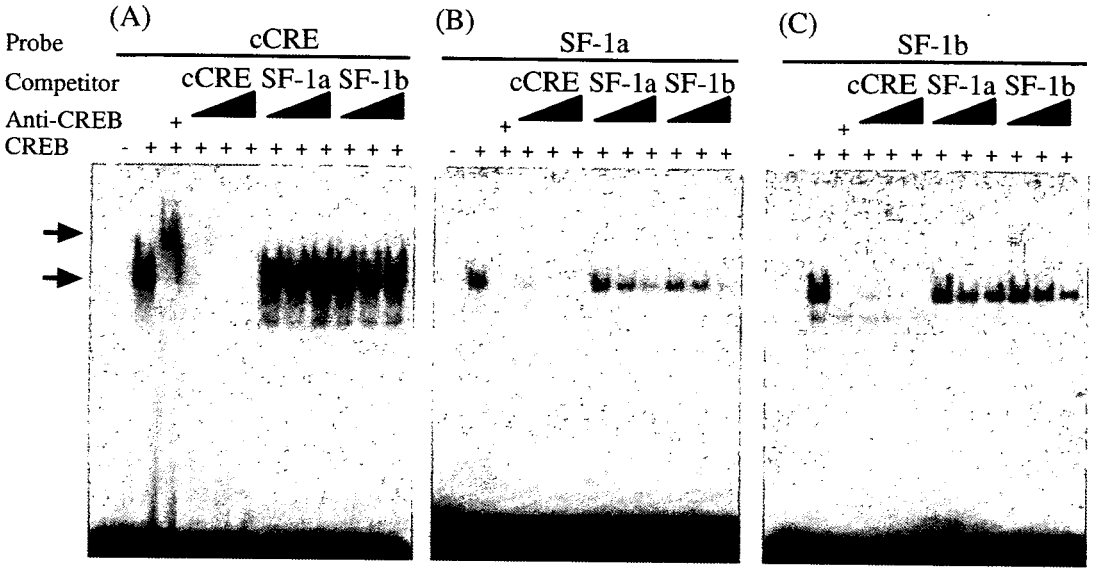

Fig. 2. **Gel shift analyses of the putative SF-1 binding sites on the human *CYP1B1* gene with CREB.** Radiolabeled cCRE (A), SF-1a (B), and SF-1b (C) were used as probes and each cold oligonucleotide was used as a competitor at 200-, 500-, and 1,000-fold molar excesses. For super-shift analyses, mouse anti-human CREB antibodies were pre-incubated with *in vitro* translated CREB protein on ice for 15 min, and then the radiolabeled probe was added. DNA-protein complexes were separated under nondenaturing conditions in 4% polyacrylamide gels. The lower arrow indicates the position of the CREB-dependent shifted band and the upper arrow indicates the super-shifted CREB complex.

(CRE: TGACGTCA), suggesting possible binding of CREB. To investigate whether CREB can bind to the SF-1a or SF-1b sites on the human *CYP1B1* gene, gel shift analyses were performed (Fig. 2). Using an oligonucleotide containing the consensus CRE sequence (cCRE), it was confirmed that the *in vitro* translated CREB binds to the sequence (Fig. 2A). A super-shifted band was observed with anti-CREB antibody. In contrast, no super-shifted band was observed with normal mouse IgG (data not shown). The band was competed out by cCRE when used as a cold competitor, but not by cold competitors of SF-1a and SF-1b. Using SF-1a or SF-1b as a probe, a shifted band was also observed with CREB (Figs. 2B and 2C). The shifted band was abolished with anti-CREB antibody, although no super-shifted band was observed. Thus, CREB barely binds to the putative SF-1–binding sites on the human *CYP1B1* gene.

Transcriptional Activities of the Human CYP1B1 Gene with the Co-Expression of SF-1 and PKA in KGN Cells—SF-1–dependent transcriptional regulation is known to be activated by PKA. To investigate whether SF-1 is involved in the transcriptional activation of the human *CYP1B1* gene via the putative SF-1 binding sites, luciferase assays were performed (Fig. 3). A luciferase reporter plasmid containing the 5′-flanking region from –2623 to +25 of the human *CYP1B1* gene was transiently transfected into KGN cells co-transfected with pRc/RSV-SF-1 plasmid, pCMV-PKA plasmid or in combination. Although the transcriptional activity was not affected by the co-expression of SF-1, it was significantly (5.9-fold) increased by the concomitant co-expression of SF-1 and PKA. However, the co-expression of PKA alone also produced similar transcriptional activation (6.7-fold). Using the mutated plasmids pGL3 (–2623/SF-1a mt), pGL3 (–2623/SF-1b mt), and pGL3 (–2623/SF-1a/b mt), the role of the putative SF-1 binding sites in the transcriptional activities was determined. The mutations did not affect the transcriptional activities in either the basal or PKA-dependent activities. These results suggest that the SF-1a and SF-1b sequences do not function in the transcriptional regulation of the human *CYP1B1* gene.

A series of deleted pGL3 plasmids were transfected into KGN cells co-transfected with the SF-1–expression vector in the absence or presence of the PKA-expression vector (Fig. 3). Using the pGL3 (–1652/+25), pGL3 (–1022/+25), and pGL3 (–910/+25) plasmids, stimulation of the transcriptional activities by PKA was observed in each plasmid (6.0-, 4.0-, and 4.9-fold, respectively), although no effects of the co-expression of SF-1 were observed (Fig. 3). Further deletion to –732 abolished the PKA-dependent transactivation. When CREB was co-expressed instead of SF-1 for each reporter construct, similar results were obtained (data not shown). These results suggest that the transcription of the human *CYP1B1* gene is regulated by PKA in the region –910 to–732.

Comparison of KGN Cells and Y-1 Cells in the Transcriptional Activities of the CYP1B1 Gene with the Co-Expression of SF-1 and PKA—As described above, SF-1 failed to transactivate the human *CYP1B1* gene. To investigate the responsiveness of SF-1 in KGN cells, a reporter plasmid containing the enhancer region of the rat *CYP1B1* gene (pFUER/0.2), which is known to be transactivated by SF-1 (*10*), was transfected (Fig. 4A). In contrast to the plasmids containing the human *CYP1B1* gene, the reporter activity of pFUER/0.2 was slightly increased by the co-expression of SF-1 (7.1-fold). Furthermore, the concomitant co-expression of SF-1 and PKA produced a maximum

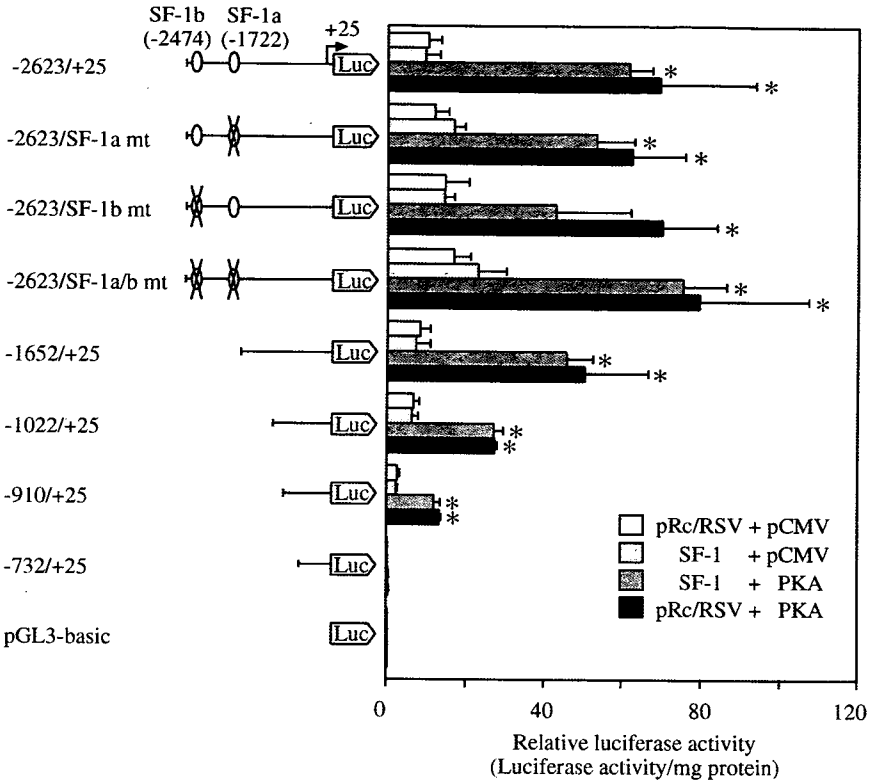

Fig. 3. **Transcriptional activity of the human *CYP1B1* gene in KGN cells.** A series of reporter constructs containing the 5′-flanking region of the human *CYP1B1* gene were transiently transfected into KGN cells with pRc/RSV-SF-1 plasmid (SF-1), pCMV-PKA plasmid (PKA), or in combination. To adjust the total amount of transfected plasmid, an empty vector (pRc/RSV or pCMV) was transfected as a control. After 48 h, luciferase activity and protein content were determined for the harvested cellular extracts. Relative luciferase activities are expressed as luciferase activity per mg protein. Each column represents the mean ± SD of three independent experiments $*P < 0.05$, compared with control (pRc/RSV and pCMV vector co-transfection).

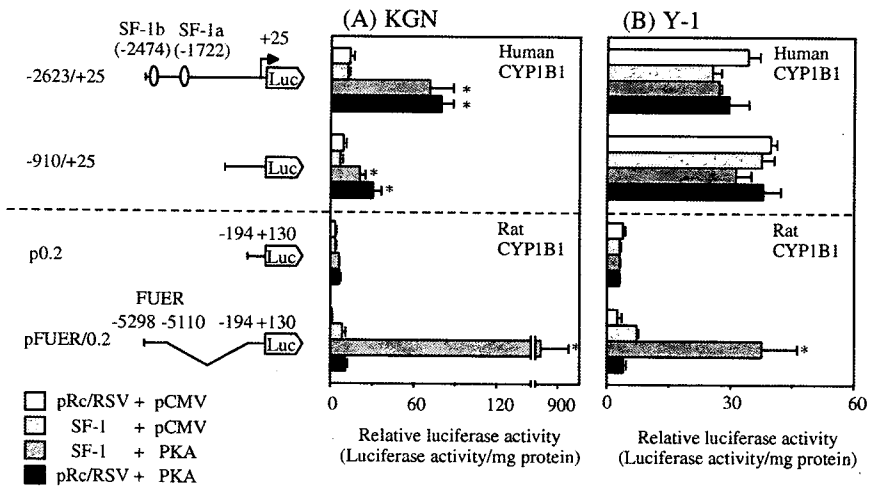

Fig. 4. **Transcriptional activity of the human or rat *CYP1B1* gene in KGN or Y-1 cells.** The reporter plasmids were pGL3 (–2623/+25) and pGL3 (–910/+25) containing the 5′-flanking region of the human *CYP1B1* gene, as well as pFUER/0.2 and p0.2 containing the 5′-flanking region of the rat *CYP1B1* gene. These reporter plasmids were transiently transfected into KGN cells (A) and Y-1 cells (B) with pRc/RSV-SF-1 plasmid (SF-1), pCMV-PKA plasmid (PKA), or in combination. To adjust the total amount of transfected plasmid, an empty vector (pRc/RSV or pCMV) was transfected as a control. After 48 h, the luciferase activity and protein content were determined for the harvested cellular extracts. Relative luciferase activities are expressed as luciferase activity per mg protein. Each column represents the mean ± SD of three independent experiments $*P < 0.05$, compared with control (pRc/RSV and pCMV vector co-transfection).

transcriptional activation of 697-fold. The reporter activity of the p0.2 construct was not affected by the co-expression of SF-1. These results suggest that SF-1 can function in KGN cells.

Mouse adrenal tumor Y-1 cells are frequently used for the examination of SF-1–regulated transactivation of target genes. Therefore, the SF-1-dependent transactivation of the human *CYP1B1* gene was investigated using Y-1

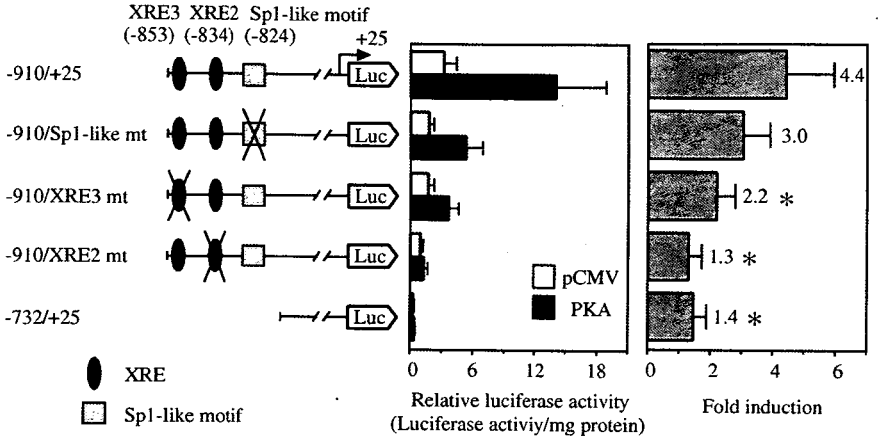

Fig. 5. **Effects of mutations of XRE3, XRE2, and the Sp1-like motif in the 5′-flanking region of the human *CYP1B1* gene on the transcriptional activity by PKA.** A series of reporter plasmids were transiently transfected into KGN cells with the pCMV-PKA plasmids. To adjust the total amount of transfected plasmid, the pCMV vector was transfected as a control. After 48 h, the luciferase activity and protein content were determined for the harvested cellular extracts. Relative luciferase activities are expressed as luciferase activity per mg protein. Constitutive and PKA-inducible transcriptional activities were demonstrated (left panel), and fold induction by PKA over control in each reporter construct was demonstrated (right panel). Each column represents the mean ± SD of three independent experiments $*P < 0.05$, compared with pGL3 (–910/+25).

cells (Fig. 4B). In accordance with the previous report (*10*), the reporter activity of pFUER was increased by the co-expression of SF-1 (2.9-fold) and concomitant co-expression of SF-1 and PKA (15-fold). In contrast, reporter plasmids containing the human *CYP1B1* gene were not transactivated by the co-expression SF-1 or PKA in Y-1 cells. These results suggest that the regulation of the rat and human *CYP1B1* genes by SF-1 is not similar.

PKA-Dependent Transactivation Is Mediated by XRE— The *CYP1B1* gene is well known to be regulated by a ligand-activated aryl hydrocarbon receptor (AhR) *via* the xenobiotic responsive element (XRE). In our previous study (*24*), it was demonstrated that two XRE sequences at –853 and –834 on the 5′-flanking region of *CYP1B1* gene cooperatively regulate the constitutive and ligand-inducible transcriptional regulation of *hCYP1B1* with the Sp1-like motif at –824. To examine the possibility that the PKA-dependent transactivation is associated with these elements, luciferase analyses with mutated reporter constructs were performed (Fig. 5). The constitutive activities of the mutated reporter plasmids pGL3 (–910/Sp1-like mt), pGL3 (–910/XRE3 mt), and pGL3 (–910/XRE2 mt) were 56%, 52%, and 30% that of wild-type pGL3 (–910/+25), respectively. The reporter activities of pGL3 (–910/+25) and pGL3 (–910/Sp1-like mt) were induced 4.4-fold and 3.0-fold by the co-transfection of PKA, respectively. In contrast, mutations in XRE3 and XRE2 significantly reduced the PKA-dependent transactivation to 2.2-fold and 1.3-fold, respectively, and the PKA-dependent transactivation was not observed with the pGL3 (–732/+25) plasmid (1.4-fold). These results suggest that the PKA-dependent transcription of the human *CYP1B1* gene is mediated by XRE3 and XRE2.

DISCUSSION

Steroidogenic CYPs such as CYP11A1 (*16*), CYP11B1 (*17*), CYP17 (*18*), and CYP19 (*19*) possess a common cAMP responsive enhancer region in the 5′-flanking region of the genes. These are regulated by SF-1 and/or CREB (*26*). It has been reported that PKA directly phosphorylates SF-1 (*27*). It was recently reported that PKA phosphorylates mitogen-activated protein kinase phosphatase-1 (MKP-1), which dephosphorylates SF-1 (*28*). Although the functions of the phosphorylation and/or dephosphorylation of SF-1 are controversial, the involvement of PKA in the activation of SF-1 would be plausible. CREB can bind to the target gene after the phosphorylation by PKA, which is activated by cAMP (*29*). CYP1B1 is also highly expressed in steroidogenic tissues such as ovary and adrenal gland, and acts in the metabolism of 17β-estradiol. It has been reported that rat CYP1B1 is regulated by SF-1 and CREB (*9*, *10*). In the present study, we investigated the possibility that SF-1 or CREB might be involved in the transcriptional regulation of the human *CYP1B1* gene.

The binding of SF-1 and CREB to two SF-1 binding sites (SF-1a and SF-1b) on the human *CYP1B1* gene was demonstrated by gel shift analyses. However, luciferase analyses revealed no transactivation of the human *CYP1B1* gene with SF-1. A similar phenomenon has been reported for human CYP11B2, aldosterone synthase, expressed in adrenal zona glomerulosa (*30*). Although SF-1 binds to the Ad4 sequence on the promoter region of the *CYP11B2* gene, SF-1 does not stimulate the transcriptional activity. Thus, if the binding affinity of SF-1 and CREB to DNA is low, these factors might be unable to transactivate.

In the rat *CYP1B1* gene, two potential CREs to which CREB can bind were identified at –5122 and –5255 (*9*). Furthermore, four SF-1 binding elements to which SF-1 can bind were identified at –5298 to –5110 (Far Upstream Enhancer Region, FUER) of the rat *CYP1B1* gene (*10*). Zheng and Jefcoate (*10*) also reported that SF-1 and CREB cooperatively transactivate the rat *CYP1B1* gene. In the present study, the SF-1– and PKA-dependent transactivation of the rat *CYP1B1* gene, but not the human *CYP1B1* gene, was observed in both KGN cells and Y-1

cells. When the sequences of the human and rat *CYP1B1* genes are compared, the homology is greater than 90% in the 5′-flanking region −1058 to −802 containing XRE. Since both the human and rat *CYP1B1* genes are up-regulated by AhR *via* XRE, this region is critical for human and rat *CYP1B1* gene regulation. However, far from −1 kbp in the 5′-flanking region, the homology between the human and rat *CYP1B1* genes decreases prominently, and the corresponding FUER rat homolog (−5298/−5110) is not found in the human *CYP1B1* gene. In the present study, we focused on two putative SF-1 binding sites at −1722 and −2474 in the *hCYP1B1* gene. Although rat FUER has multiple binding regions for SF-1 and CREB in a short sequence (189 bp), the SF-1a and SF-1b sites in the human *CYP1B1* gene exist separately. Thus, the dissimilarity in the sequences in the regulatory regions of the human and rat *CYP1B1* genes might be the cause of the low contribution of SF-1 to the regulation of the human *CYP1B1* gene. Taking our present data into consideration, SF-1 would not be a major regulator of human CYP1B1 expression. However, we cannot exclude the possibility that SF-1 might act indirectly if SF-1 modifies another transcriptional factor(s) that regulates human CYP1B1.

We found that PKA activates the transcription between −910 to −732 on the 5′-flanking region of the human *CYP1B1* gene (Fig. 3). This region includes two XRE sites and an Sp1-like motif, which play roles in the regulation of *CYP1B1* in constitutive and AhR-ligand dependent expression (*24*). It is well known that AhR binds to XRE after heterodimerization with AhR nuclear translocator (ARNT) (*31*, *32*). Interestingly, mutations in XRE3 at −853 and XRE2 at −834 inhibit the PKA-dependent activation (Fig. 5). As shown in Fig. 4, this PKA-dependent transactivation of the human *CYP1B1* gene was observed in KGN cells, but not in Y-1 cells. In KGN cells, AhR mRNA is expressed and can induce the CYP1B1 mRNA in the presence of ligands (data not shown). In contrast, AhR mRNA is not expressed in Y-1 cells (*9*). Thus, AhR is likely to be involved in PKA-dependent transactivation. A number of early studies reported the phosphorylation of AhR; especially, the phosphorylation of AhR via protein kinase C (PKC) is well known to be essential for the binding of AhR to XRE (*33*, *34*). Until now, the association of PKA with the phosphorylation of AhR activation was unknown. However, it has been reported that PKA augments the transactivation potential of ARNT, a partner of AhR (*35*). The findings of our study suggest that the PKA signaling pathway is partially involved in the transcriptional regulation of the human *CYP1B1* gene *via* XRE, although further studies are necessary.

In conclusion, we demonstrated the binding of SF-1 and CREB to the putative SF-1 binding sites of the human *CYP1B1* gene, but these factors do not activate transcription. Thus, SF-1 and CREB might not be essential for the regulation of the human *CYP1B1* gene. Interestingly, it was found that PKA signaling is involved in the XRE-mediated transactivation in the human *CYP1B1* gene.

We are grateful to Dr. Ken-ichirou Morohashi of the National Institute for Basic Biology (Okazaki, Japan) for providing the pRc/RSV-SF-1 plasmid and anti–SF-1 serum. We also thank Drs. Yoshihiro Nishi, Toshihiko Yanase, and Hajime Nawata of Kyushu University (Fukuoka, Japan) for providing the KGN cells. We acknowledge Mr. Brent Bell for reviewing the manuscript. This work was supported in part by Research on Advanced Medical Technology, Health and Labor Science Research Grants from the Ministry of Health, Labor and Welfare of Japan.

REFERENCES

1. Gonzalez, F.J. (1988) The molecular biology of cytochrome P450s. *Pharmacol. Rev.* **40**, 243–288
2. Guengerich, F.P. and Shimada, T. (1991) Oxidation of toxic and carcinogenic chemicals by human cytochrome P-450 enzymes. *Chem. Res. Toxicol.* **4**, 391–407
3. Sutter, T.R., Tang, Y.M., Hayes, C.L., Wo, Y-Y.P., Jabs, E.W., Li, X., Yin, H., Cody, C.W., and Greenlee, W.F. (1994) Complete cDNA sequence of a human dioxin-inducible mRNA identifies a new gene subfamily of cytochrome P450 that maps to chromosome 2. *J. Biol. Chem.* **269**, 13092–13099
4. Shimada, T., Hayes, C.L., Yamazaki, H., Amin, S., Hecht, S.S., Guengerich, F.P., and Sutter, T.R. (1996) Activation of chemically diverse procarcinogens by human cytochrome P450 1B1. *Cancer Res.* **56**, 2979–2984
5. Hayes, C., Spink, D., Spink, B., Cao, J., Walker, N., and Sutter, T. (1996) 17β-Estradiol hydroxylation catalyzed by human cytochrome P450 1B1. *Proc. Natl. Acad. Sci. USA* **93**, 9776–9781
6. Spink, D.C., Spink, B.C., Cao, J.Q., Gierthy, J.F., Hayes, C.L., Li, Y., and Sutter, T.R. (1997) Induction of cytochrome P450 1B1 and catechol estrogen metabolism in ACHN human renal adenocarcinoma cells. *J. Steroid. Biochem. Mol. Biol.* **62**, 223–232
7. Bhattacharyya, K.K., Brake, P.B., Eltom, S.E., Otto, S.A., and Jefcoate, C.R. (1995) Identification of a rat adrenal cytochrome P450 active in polycyclic hydrocarbon metabolism as rat CYP1B1. Demonstration of a unique tissue-specific pattern of hormonal and aryl hydrocarbon receptor-linked regulation. *J. Biol. Chem.* **270**, 11595–11602
8. Brake, P.B. and Jefcoate, C.R. (1995) Regulation of cytochrome P4501B1 in cultured rat adrenocortical cells by cyclic adenosine 3′,5′-monophosphate and 2,3,7,8-tetrachlorodibenzo-*p*-dioxin. *Endocrinology* **136**, 5034–5041
9. Zheng, W., Brake, P.B., Bhattacharyya, K.K., Zhang, L., Zhao, D., and Jefcoate, C.R. (2003) Cell selective cAMP induction of rat *CYP1B1* in adrenal and testis cells. Identification of a novel cAMP-responsive far upstream enhancer and a second Ah receptor-dependent mechanism. *Arch. Biochem. Biophys.* **416**, 53–67
10. Zheng, W. and Jefcoate, C.R. (2005) Steroidogenic factor-1 interacts with cAMP response element-binding protein to mediate cAMP stimulation of *CYP1B1* via a far upstream enhancer. *Mol. Pharmacol.* **67**, 499–512
11. Ikeda, Y., Lala, D.S., Luo, X., Kim, E., Moisan, M.P., and Parker, K.L. (1993) Characterization of the mouse FTZ-F1 gene, which encodes a key regulator of steroid hydroxylase gene expression. *Mol. Endocrinol.* **7**, 852–860
12. Morohashi, Ki. (1999) Gonadal and extragonadal functions of Ad4BP/SF-1: developmental aspects. *Trends Endocrinol. Metab.* **10**, 169–173
13. Luo, X., Ikeda, Y., Lala, D.S., Baity, L.A., Meade, J.C., and Parker, K.L. (1995) A cell-specific nuclear receptor plays essential roles in adrenal and gonadal development. *Endocr. Res.* **21**, 517–524
14. Luo, X., Ikeda, Y., Parker, K.L. (1994) A cell-specific nuclear receptor is essential for adrenal and gonadal development and sexual differentiation. *Cell* **77**, 481–490
15. Sugawara, T., Holt, J.A., Kiriakidou, M., and Strauss III, J.F. (1996) Steroidogenic factor 1-dependent promoter activity of the human steroidogenic acute regulatory protein (StAR) gene. *Biochemistry* **35**, 9052–9059

16. Hu, M.C., Hsu, N.C., Pai, C.I., Wang, C.K., and Chung, B.C. (2001) Functions of the upstream and proximal steroidogenic factor 1 (SF-1)-binding sites in the *CYP11A1* promoter in basal transcription and hormonal response. *Mol. Endocrinol.* **15**, 812–818
17. Wang, X.L., Bassett, M., Zhang, Y., Yin, S., Clyne, C., White, P.C., and Rainey, W.E. (2000) Transcriptional regulation of human 11β-hydroxylase (*hCYP11B1*). *Endocrinology* **141**, 3587–3594
18. Hanley, N.A., Rainey, W.E., Wilson, D.I., Ball, S.G., and Parker, K.L. (2001) Expression profiles of SF-1, DAX1, and CYP17 in the human fetal adrenal gland: potential interactions in gene regulation. *Mol. Endocrinol.* **15**, 57–68
19. Michael, M.D., Kilgore, M.W., Morohashi, K., and Simpson, E.R. (1995) Ad4BP/SF-1 regulates cyclic AMP-induced transcription from the proximal promoter (PII) of the human aromatase P450 (*CYP19*) gene in the ovary. *J. Biol. Chem.* **270**, 13561–13566
20. Morohashi, K., Honda, S., Inomata, Y., Handa, H., and Omura, T. (1992) A common *trans*-acting factor, Ad4-binding protein, to the promoters of steroidogenic P-450s. *J. Biol. Chem.* **267**, 17913–17919
21. Andrisani, O.M., (1999) CREB-mediated transcriptional control. *Crit. Rev. Eukaryot. Gene Expr.* **9**, 19–32
22. Ito, M., Park, Y., Weck, J., Mayo, K.E., and Jameson, J.L. (2000) Synergistic activation of the inhibin α-promoter by steroidogenic factor-1 and cyclic adenosine 3′,5′-monophosphate. *Mol. Endocrinol.* **14**, 66–81
23. Yazawa, T., Mizutani, T., Yamada, K., Kawata, H., Sekiguchi, T., Yoshino, M., Kajitani, T., Shou, Z., and Miyamoto, K. (2003) Involvement of cyclic adenosine 5′-monophosphate response element-binding protein, steroidogenic factor 1, and Dax-1 in the regulation of gonadotropin-inducible ovarian transcription factor 1 gene expression by follicle-stimulating hormone in ovarian granulosa cells. *Endocrinology* ***144, 1920–1930***
24. Tsuchiya, Y., Nakajima, M., and Yokoi, T. (2003) Critical enhancer region to which AhR/ARNT and Sp1 bind in the human *CYP1B1* gene. *J. Biochem.* **133**, 583–592
25. Nishi, Y., Yanase, T., Mu, Y., Oba, K., Ichino, I., Saito, M., Nomura, M., Mukasa, C., Okabe, T., Goto, K., Takayanagi, R., Kashimura, Y., Haji, M., and Nawata, H. (2001) Establishment and characterization of a steroidogenic human granulosa-like tumor cell line, KGN, that expresses functional follicle-stimulating hormone receptor. *Endocrinology* **142**, 437–445
26. Val, P., Lefrancois-Martinez, A.M., Veyssiere, G., and Martinez, A. (2003) SF-1 a key player in the development and differentiation of steroidogenic tissues. *Nucl. Recept.* **1**, 8
27. Zhang, P. and Mellon, S.H. (1996) The orphan nuclear receptor steroidogenic factor-1 regulates the cyclic adenosine 3′,5′-monophosphate-mediated transcriptional activation of rat cytochrome P450c17 (17α-hydroxylase/c17–20 lyase). *Mol. Endocrinol.* **10**, 147–158
28. Sewer, M.B. and Waterman, M.R. (2003) cAMP-dependent protein kinase enhances CYP17 transcription via MKP-1 activation in H295R human adrenocortical cells. *J. Biol. Chem.* **278**, 8106–8111
29. Don, J. and Stelzer, G. (2002) The expanding family of CREB/CREM transcription factors that are involved with spermatogenesis. *Mol. Cell. Endocrinol.* **187**, 115–124
30. Bassett, M.H., Zhang, Y., Clyne, C., White, P.C., and Rainey, W.E. (2002) Differential regulation of aldosterone synthase and 11β-hydroxylase transcription by steroidogenic factor-1. *J. Mol. Endocrinol.* **28**, 125–135
31. Hankinson, O. (1995) The aryl hydrocarbon receptor complex. Annu. *Rev. Pharmacol. Toxicol.* **35**, 307–340
32. Schmidt, J.V. and Bradfield, C.A. (1996) Ah receptor signaling pathways. *Annu. Rev. Cell. Biol.* **12**, 55–89
33. Berghard, A., Gradin, K., Pongratz, I., Whitelaw, M., and Poellinger, L. (1993) Cross-coupling of signal transduction pathways: the dioxin receptor mediates induction of cytochrome P-450IA1 expression via a protein kinase C-dependent mechanism. *Mol. Cell. Biol.* **13**, 677–689
34. Long, W.P., Pray-Grant, M., Tsai, J.C., and Perdew, G.H. (1998) Protein kinase C activity is required for aryl hydrocarbon receptor pathway-mediated signal transduction. *Mol. Pharmacol.* **53**, 691–700
35. Long, W.P., Chen, X., and Perdew, G.H. (1999) Protein kinase C modulates aryl hydrocarbon receptor nuclear translocator protein-mediated transactivation potential in a dimer context. *J. Biol. Chem.* **274**, 12391–12400

Kinetic Analyses for Species Differences in P-glycoprotein-Mediated Drug Transport

MIKI KATOH,[1] NAOTO SUZUYAMA,[1] TOSHIYUKI TAKEUCHI,[2] SUMIE YOSHITOMI,[2] SATORU ASAHI,[2] TSUYOSHI YOKOI[1]

[1]Drug Metabolism and Toxicology, Division of Pharmaceutical Sciences, Graduate School of Medical Science, Kanazawa University, Kakuma-machi, Kanazawa 920-1192, Japan

[2]Pharmaceutical Research Division, Takeda Pharmaceutical Company Ltd., Osaka, Japan

Received 22 March 2006; revised 1 May 2006; accepted 7 May 2006

Published online in Wiley InterScience (www.interscience.wiley.com). DOI 10.1002/jps.20686

ABSTRACT: P-glycoprotein (P-gp) plays an important role in the pharmacokinetics of drugs. There is little information on the species differences in P-gp-mediated drug transport activity. The purpose of the present study was to clarify the differences in the kinetic parameters and the existence of species differences in the P-gp-mediated drug transport activity using seven *multidrug resistence1* (*MDR1*) transfected cell lines, in which the cDNA was from human, monkey, canine, rat (*MDR1a* and *MDR1b*), and mouse (*mdr1a* and *mdr1b*). The transcellular transport of diltiazem, cyclosporin A, and dexamethasone across monolayers of *MDR1* transfected cells. The apparent K_m values of diltiazem exhibited approximately 16.5-fold differences among the seven cell lines. Concerning the diltiazem transport, the V_{max}/K_m value of human P-gp corrected by the P-gp expression level was similar to that of monkey P-gp, but was 5.6-fold higher than that of canine P-gp. On the other hand, the corrected V_{max}/K_m value of human P-gp for cyclosporin A transport was 3.8-fold higher than that of monkey P-gp. The present study would be valuable to evaluate the P-gp function of various animals in the same experimental condition. It was clarified that the species differences in P-gp-mediated drug transport activity evaluated by the corrected V_{max}/K_m value differed according to the substrate. © 2006 Wiley-Liss, Inc. and the American Pharmacists Association J Pharm Sci 95:2673–2683, 2006

Keywords: multidrug resistance transporters; P-glycoprotein; species differences; kinetics; drug transport; *in vitro* models

INTRODUCTION

P-glycoprotein (P-gp) is a product of *multidrug resistant* 1 (*MDR1*) gene and is one of the most important transporters affecting the pharmacokinetics of drugs in normal cells as well as in cancer cells. A rational approach is needed to determine whether a compound is a P-gp substrate or not, especially in drug development. The Caco-2 cells and human *MDR1* transfected cell lines such as LLC-GA5-COL150 and L-MDR1 established by Ueda et al.[1] and Schinkel et al.,[2] respectively, are frequently used for *in vitro* P-gp assays. On the other hand, the P-gp function has been evaluated using gene knockout mice, *mdr1a*$^{-/-}$, *mdr1b*$^{-/-}$, and double knockout *mdr1a*$^{-/-}$/*mdr1b*$^{-/-}$ mice.[3,4] The *in vivo* brain concentration ratio for *mdr1a*$^{-/-}$ and wild-type mice correlated with the *in vitro* basolateral (B)-to-apical (A)/A-to-B transport ratio in L-mdr1a cells, which are transfected with mouse *mdr1a* gene, suggesting that *in vitro* data could predict the *in vivo* contribution of P-gp.[5] Concerning

Correspondence to: Tsuyoshi Yokoi (Telephone: +81-76-234-4407; Fax: +81-76-234-4407;
E-mail: TYOKOI@kenroku.kanazawa-u.ac.jp)

Journal of Pharmaceutical Sciences, Vol. 95, 2673–2683 (2006)

species differences in the P-gp function, the correlation between the data using L-MDR1 cells *in vitro* and those of mice *in vivo* was weak compared with that between *in vitro* data using L-mdr1a cells and mice *in vivo*. The functions of human and mouse P-gp were different in terms of the drug resistance and the sensitivity to modulators.[6] For 642 structurally diverse compounds, the correlation between transcellular transport activities across monolayers of L-MDR1 and L-mdr1a cell lines was poor.[7] However, Adachi et al.[8] reported that there were minimal species differences in the substrate recognition by P-gp between human and mice using a human *MDR1* transfected LLC-PK_1 cell line and *mdr1a*$^{-/-}$/*mdr1b*$^{-/-}$ mice, although the number of test drugs was small. There have been few comparisons of the P-gp function between human and other animals. Species differences in the P-gp-mediated drug transport activity are not fully understood.

Recently, Takeuchi et al.[9] established various *MDR1* transfected cell lines designated as hMDR1 (human *MDR1*), pMDR1 (monkey *MDR1*), cMDR1 (canine *MDR1*), rMDR1a (rat *MDR1a*), rMDR1b (rat *MDR1b*), mmdr1a (mouse *mdr1a*), and mmdr1b (mouse *mdr1b*), which stably express the P-gp encoded by each gene. These cell lines were clarified to have potency in the transport of P-gp substrates.[9] The purpose of the present study is to clarify the species differences in P-gp-mediated drug transport with kinetic analyses using these P-gp expressing cells in the same experimental system. The transport of typical P-gp substrates was determined and obvious species differences depending on the substrate were demonstrated by kinetic analyses.

MATERIALS AND METHODS

Materials

[*mebmt*-β-^{3}H]Cyclosporin A (333.0 GBq/mmol) and [1,2,4-^{3}H]dexamethasone (1480.0 GBq/mmol) were obtained from Amersham Biosciences (Buckinghamshire, UK). *cis*-(+)-[*N*-methyl-^{3}H] Diltiazem (3145.0 GBq/mmol) was purchased from PerkinElmer Life Sciences (Boston, MA). Colchicine, cyclosporin A, dexamethasone, and diltiazem hydrochloride were obtained from Wako Pure Chemical Industries (Osaka, Japan). The mouse monoclonal antibodies (C219) and rabbit polyclonal antibodies (H241) against *MDR1*-encoded P-gp were purchased from Calbiochem (San Diego, CA) and Santa Cruz Biotechnology (Santa Cruz, CA), respectively. The biotinylated secondary antibodies against mouse and rabbit were from Invitrogen (Carlsbad, CA) and Vector laboratories (Burlingame, CA), respectively. All other materials were of the highest purity available.

Cell Culture

The hMDR1, pMDR1, cMDR1, rMDR1a, rMDR1b, mmdr1a, and mmdr1b cell lines, in which each *MDR1* gene was transfected into LLC-PK_1 cells, and a mock cell line were established by Takeuchi et al.[9] The mock cell line was transfected with an empty vector into LLC-PK_1 cells. The conditions of the cell culture were described previously.[9] Briefly, all *MDR1* transfected cells and mock cells were incubated in complete medium consisting of Medium 199 (Nissui Pharmaceutical, Tokyo, Japan) with 10% fetal bovine serum (Trace Scientific, Melbourne, Australia) and 500 μg/mL G418 (MP Biomedicals, Irvine, CA). For *MDR1* transfected cells, 150 ng/mL of colchicine was added in the medium. A monolayer culture was grown in an atmosphere of 5% CO_2 to 95% air at 37°C.

Immunoblot Analysis of P-gp on *MDR1* Transfected Cells

Sodium dodecyl sulfate-polyacrylamide gel electrophoresis and immunoblot analysis of P-gp were performed using homogenates of cells according to the method of Laemmli[10] with slight modifications. Four days after the confluence, the cells were washed with phosphate-buffered saline (PBS) and scraped off the dishes. The pellet of cells was homogenized in ice-cold PBS containing 1 mM (*p*-amidinophenyl)methanesulfonyl fluoride, 1 μg/mL aprotinin, 1 μg/mL pepstatin, 1 μg/mL leupeptin, and 1 mM dithiothreitol. The protein concentration was determined using Bradford protein assay reagent (Bio-Rad, Hercules, CA) with bovine gamma globulin as a standard. The total of 50 μg protein obtained from the cells was separated on 7.5% polyacrylamide gel and transferred electrophoretically to a polyvinylidene difluoride membrane. After blocking, the membrane was incubated with C219 or H241 antibodies. Biotinylated anti-rabbit or mouse IgG and a Vectastain ABC kit (Vector Laboratories) were used for diaminobenzidine staining.

DOI 10.1002/jps

Transcellular Transport

The experiments were performed according to the procedure described previously[11] with slight modifications. The *MDR1* transfected cells and mock cells were seeded on microporous polycarbonate membrane filters (Transwell™, 3402, Corning, Acton, MA) at a cell density of 7.5×10^5 cells/cm^2. Cells were cultured on a membrane filter with 1.5 and 0.5 mL of the complete medium in the outside and inside of the chamber, respectively, in an atmosphere of 5% CO_2 to 95% air at 37°C for 4 days. Fresh medium was replaced on the second day and fresh medium without G418 and colchicine was replaced on the third day after seeding. In the present study, *MDR1* transfected cells and mock cells were used between passages 8 and 33 (hMDR1), 5 and 33 (pMDR1), 7 and 34 (cMDR1), 5 and 31 (rMDR1a), 7 and 32 (rMDR1b), 6 and 31 (mmdr1a), 11 and 34 (mmdr1b), and 45 and 47 (mock), respectively. Three hours before the start of the experiment, all culture media were replaced with fresh medium with neither G418 nor colchicine. The medium on the donor side of the monolayers was replaced with that containing unlabeled diltiazem with 1.1 nM *cis*-(+)-[*N*-methyl-^{3}H]diltiazem (3.5 kBq/mL), unlabeled cyclosporin A with 38.3 nM [*mebmt*-β-^{3}H]cyclosporin A (12.8 kBq/mL), or unlabeled dexamethasone with 9.4 nM [1,2,4-^{3}H]dexamethasone (13.9 kBq/mL). The unlabeled cyclosporin A and dexamethasone were dissolved in dimethylsulfoxide. For the evaluation of the kinetic parameters, the concentrations of diltiazem, cyclosporin A, and dexamethasone ranged from 1 to 50, 0.5 to 20, and 100 to 1000 μM, respectively. The final concentration of the solvent in the media was <1% (v/v) except for dexamethasone (5.0%). We confirmed that 5.0% ethanol did not affect the transcellular transport and the protein contents of *MDR1* transfected cells and that high concentration of the substrate did not induce the cell toxicity. Aliquots from the receiver side (50 μL of inside or 150 μL of outside) were taken at 1.0 h. After the addition of 4 mL scintillation cocktail, Clear-sol I (Nacalai tesque, Kyoto, Japan), the radioactivity was measured using a liquid scintillation counter (LSC 5100, Aloka, Tokyo, Japan).

To determine the intracellular accumulation study, the cells were washed with ice-cold PBS immediately after sampling. The cells were solubilized with 0.5 mL of 0.3 M NaOH overnight, and were neutralized with 0.5 mL of 0.3 M HCl. The radioactivity of a 200 μL portion of the aliquots was measured. The protein contents of *MDR1* transfected cells and mock cells were measured using the method of Lowry et al.[12] with bovine serum albumin as a standard. The protein contents in cell monolayers ranged from 0.12 to 0.23 (hMDR1), 0.12 to 0.22 (pMDR1), 0.18 to 0.30 (cMDR1), 0.14 to 0.22 (rMDR1a), 0.11 to 0.21 (rMDR1b), 0.10 to 0.24 (mmdr1a), 0.12 to 0.25 (mmdr1b), and 0.23 to 0.36 (mock) mg/filter, respectively. The data of the transcellular transports were calculated by using more than three independent measurements.

Kinetic Study on Transcellular Transport

The amount of the transport was fitted to the Michaelis–Menten equation using a nonlinear regression analysis program (Kaleida Graph, Synergy Software, Peding, PA) to calculate the kinetic parameters.

Michaelis–Menten kinetics are described as follows:

$$V = V_{max} \cdot \frac{C_D}{K_m + C_D} \quad (1)$$

where V is defined as the net transport in the present study. To calculate the apparent K_m value, the V value in the present study was defined as V_{raw} (Eq. 2) or V_{ad} (Eq. 3).

$$V_{raw} = P_{B\text{-to-}A,\,MDR1} - P_{A\text{-to-}B,\,MDR1} \quad (2)$$

where the $P_{B\text{-to-}A,\ MDR1}$ and $P_{A\text{-to-}B,\ MDR1}$ values were obtained from the B-to-A and A-to-B directed permeability including P-gp-mediated transport and passive diffusion in *MDR1* transfected cells. The $K_{m,raw}$ and $V_{max,raw}$ values were calculated using the V_{raw} values.

$$V_{ad} = (P_{B\text{-to-}A,\,MDR1} - P_{A\text{-to-}B,\,MDR1}) - (P_{B\text{-to-}A,\,mock} - P_{A\text{-to-}B,\,mock}) \quad (3)$$

where the $P_{B\text{-to-}A,\ mock}$ and $P_{A\text{-to-}B,\ mock}$ values were obtained from the permeability in mock cells. The V_{ad} value results from subtracting the apparent net transport in mock cells from that in *MDR1* transfected cells. The $K_{m,ad}$ and $V_{max,ad}$ values were calculated using the V_{ad} values.

The $V_{max,ad}/K_{m,ad}$ values of the *MDR1* transfected cells were corrected using the expression levels of P-gp quantified by Western blot analysis using C219 antibodies. The P-gp expression level of cells was quantified relative to the P-gp expressed in hMDR1 cells.

Efflux Ratio of Transcellular Transport

The efflux ratio was calculated using Eq. (4):

$$\text{Efflux ratio} = \frac{P_{\text{B-to-A, MDR1}}}{P_{\text{A-to-B, MDR1}}} \quad (4)$$

The corrected efflux ratio was defined as Eq. (5) by Adachi et al.[8]:

$$\text{Corrected efflux ratio} = \frac{\text{efflux ratio}_{\text{MDR1}}}{\text{efflux ratio}_{\text{mock}}} = \frac{P_{\text{B-to-A, MDR1}}/P_{\text{B-to-A, mock}}}{P_{\text{A-to-B, MDR1}}/P_{\text{A-to-B, mock}}} \quad (5)$$

The efflux ratio was calculated using P values at a concentration showing linear transport. The concentrations of diltiazem, cyclosporin A, and dexamethasone were 11, 66, and 37 nM, respectively.

RESULTS

Immunoblot Analysis of *MDR1* Transfected Cells

The results of the immunoblot analysis using anti-P-gp antibodies, C219 and H241, are shown in Figure 1. In the case of the C219 antibodies, the densities of the bands from pMDR1, cMDR1, rMDR1b, and mmdr1a were higher than that from hMDR1 (Fig. 1A). The relative densities of hMDR1, pMDR1, cMDR1, rMDR1a, rMDR1b, mmdr1a, and mmdr1b were 1.0, 1.6, 2.6, 0.9, 1.6, 1.6, and 1.1, respectively. On the other hand, in the case of the H241 antibodies, the densities of the bands from pMDR1 and cMDR1 were higher, but those of rMDR1b and mmdr1a were lower than that from hMDR1 (Fig. 1B). The relative densities of hMDR1, pMDR1, cMDR1, rMDR1a, rMDR1b, mmdr1a, and mmdr1b were 1.0, 1.8, 1.5, 0.7, 0.5, 0.4, and 0.4, respectively. In the present study, the correction by the P-gp expression level was used for the result with the C219 antibodies.

Kinetic Analysis of Diltiazem Transport

The transcellular transport of diltiazem in *MDR1* transfected cells is shown in Figure 2. The changes of the V_{raw} and V_{ad} values are shown in Figure 2A–F, respectively. The corrected V_{ad} values estimated by the expression level of P-gp measured by Western blot analysis are shown in Figure 2G–I. The apparent K_m and V_{max} values are shown in Table 1. Both the apparent $K_{m,raw}$ and $K_{m,ad}$ values calculated using the V_{raw} and V_{ad} values, respectively, were similar. The apparent $K_{m,ad}$ values of pMDR1 and rMDR1a were lower than that of hMDR1. On the other hand, the apparent $K_{m,ad}$ values of cMDR1 and mmdr1b were higher than that of hMDR1. The apparent $K_{m,ad}$ values ranged from 2.1 to 34.6 μM (16.5-fold). Both $V_{max,ad}/K_{m,ad}$ and the corrected $V_{max,ad}/K_{m,ad}$ values of hMDR1 were higher than those of cMDR1. The $V_{max,ad}/K_{m,ad}$ and the corrected $V_{max,ad}/K_{m,ad}$ values of rMDR1a were high, but those of rMDR1b, mmdr1a, and mmdr1b were similar or lower than that of rMDR1a.

The efflux ratio and corrected efflux ratio of diltiazem transport at 11 nM are shown in Table 1. The efflux ratio and the corrected efflux ratio did

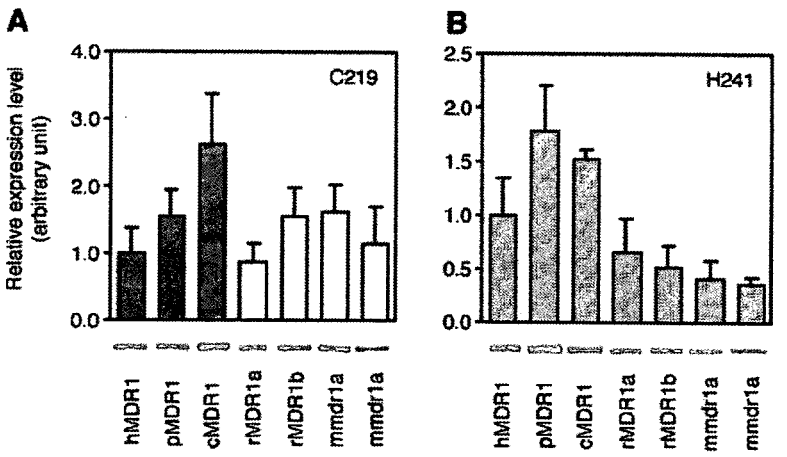

Figure 1. Immunoblot analysis of P-gp in *MDR1* transfected cells. Immunoblot analyses of P-gp expressed in *MDR1* transfected cells were performed using anti-P-gp antibodies, (A) C219 and (B) H241. Each column represents the mean ± SE of more than four determinations.

DOI 10.1002/jps

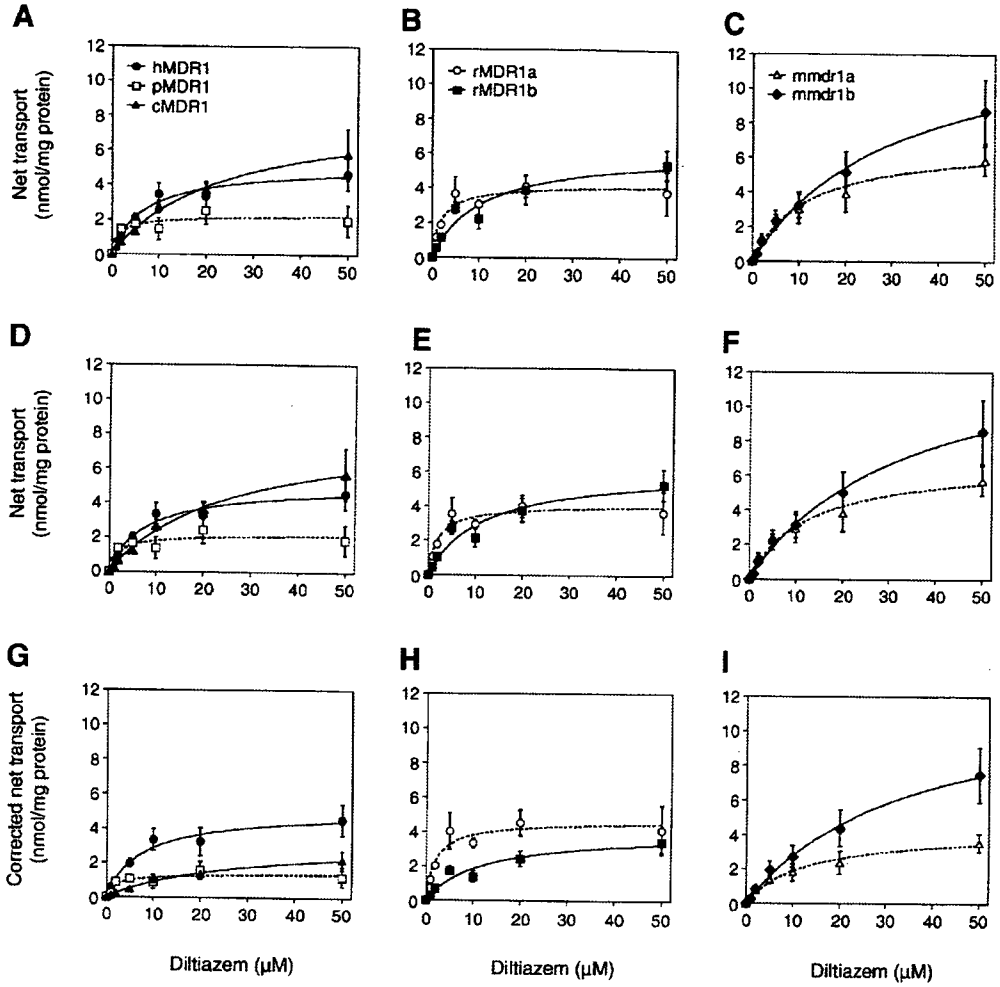

Figure 2. Net transport of diltiazem across *MDR1* transfected cells: (A–C), the net transport was shown as the V_{raw} value; (D–F), the net transport was shown as the V_{ad} value; (G–I), the net transport was shown as the corrected V_{ad} value calculated by Western blot analysis using C219 antibodies. Each point represents the mean ± SEM of more than three determinations.

not exhibit large differences among the species. As compared to the value of hMDR1, pMDR1, and rMDR1a appeared higher and mmdr1b appeared lower, but the difference was small (~1.5-fold).

Intracellular accumulations of diltiazem at 1 h form the B-to-A and A-to-B transports are shown in Figure 3A–F, respectively. The increases of the intracellular accumulations of the B-to-A and A-to-B transports showed similar patterns in the P-gp expressing cells.

Kinetic Analysis of Cyclosporin A Transport

The transcellular transport of cyclosporin A in *MDR1* transfected cells is shown in Figure 4. The corrected V_{ad} values estimated by the expression level of P-gp measured by Western blot analysis are shown in Figure 4A–C. The profiles of the V_{raw} and V_{ad} values were almost the same and the apparent $K_{m,raw}$ and $K_{m,ad}$ values calculated using the V_{raw} and V_{ad} values, respectively, were similar (data not shown). The values of $K_{m,ad}$ and $V_{max,ad}$ are shown in Table 2. The apparent $K_{m,ad}$ values of hMDR1 and pMDR1 were similar and were lower than that of mmdr1b. In cMDR1, rMDR1a, rMDR1b, and mmdr1a the net transports increased linearly up to 20 μM. Thus, we could calculate neither the V_{max} nor V_{max}/K_m values. The $V_{max,ad}/K_{m,ad}$ and corrected $V_{max,ad}/K_{m,ad}$ values of hMDR1 were higher than those of

Table 1. Kinetic Parameters and Efflux Ratio of Diltiazem Transport across Monolayers of *MDR1* Transfected Cells

Cell Line	$K_{m,raw}$[a] (μM)	$K_{m,ad}$[b] (μM)	$V_{max,raw}$[a] (nmol/mg/h)	$V_{max,ad}$[b] (nmol/mg/h)	$V_{max,ad}/K_{m,ad}$ (mL/mg/h)	Corrected $V_{max,ad}/K_{m,ad}$[c] (mL/mg/h)	Efflux Ratio[d]	Corrected Efflux Ratio[d]
hMDR1	7.0	7.6	5.1	5.6	0.67	0.67	2.5	2.5
pMDR1	1.9	2.1	2.2	2.2	1.02	0.65	3.2	3.0
cMDR1	23.8	26.2	8.5	8.6	0.33	0.12	2.5	2.4
rMDR1a	2.0	2.2	4.2	4.1	1.88	2.14	3.0	2.8
rMDR1b	10.5	11.6	6.2	6.2	0.53	0.34	2.1	1.9
mmdr1a	11.7	12.8	6.9	6.9	0.54	0.33	2.7	2.5
mmdr1b	32.0	34.6	14.0	14.3	0.41	0.36	1.7	1.6

[a]The $K_{m,raw}$ and $V_{max,raw}$ values estimated using the V_{raw} value described as Eq. 2 in Materials and Methods.
[b]The $K_{m,ad}$ and $V_{max,ad}$ values estimated using the V_{ad} value described as Eq. 3 in Materials and Methods.
[c]The corrected $V_{max,ad}/K_{m,ad}$ value calculated using the corrected $V_{max,ad}$ value, which was obtained by taking the relative expression level of P-gp measured by Western blot analysis using C219 antibodies into consideration.
[d]Efflux ratio and corrected efflux ratio were estimated as Eqs. 4 and 5, respectively, as described in Materials and Methods. Efflux ratio was calculated at 11 nM diltiazem.

pMDR1. As compared to the diltiazem transport, the relative values of $K_{m,ad}$, $V_{max,ad}$, and $V_{max,ad}/K_{m,ad}$ in *MDR1* transfected cells toward hMDR1were different from those of cyclosporin A.

The efflux ratio and corrected efflux ratio of cyclosporin A transport at 66 nM are also shown in Table 2. The efflux ratio and the corrected efflux ratio were different. In hMDR1, the $P_{B\text{-to-}A,\ MDR1}$ and $P_{A\text{-to-}B,\ MDR1}$ values were 10.4 ± 1.67 and 0.55 ± 0.06 pmol/mg protein/h, respectively. In mock cells, the $P_{B\text{-to-}A,\ mock}$ and $P_{A\text{-to-}B,\ mock}$ values were 1.38 ± 0.08 and 0.51 ± 0.07 pmol/mg protein/h, respectively. As compared to the $P_{B\text{-to-}A,\ MDR1}$ value, the $P_{B\text{-to-}A,\ mock}$ value was low, but the efflux ratio in mock cells was calculated as 2.7 at 66 nM cyclosporin A. The efflux ratio and the corrected efflux ratio in cMDR1 were lower than those in hMDR1. Both the efflux ratio and the corrected

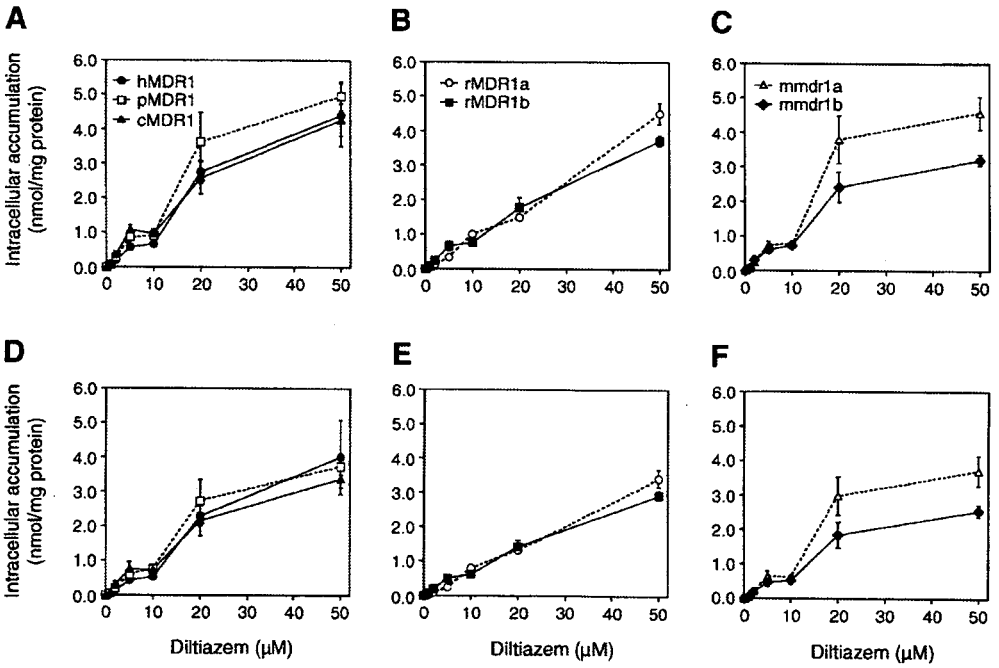

Figure 3. Intracellular accumulation of diltiazem in *MDR1* transfected cells: (A–C), the intracellular accumulation of diltiazem resulting from BA transport at 1 h; (D–F), the intracellular accumulation of diltiazem resulting from AB transport at 1 h. Each point represents the mean ± SEM of more than three determinations.

DOI 10.1002/jps

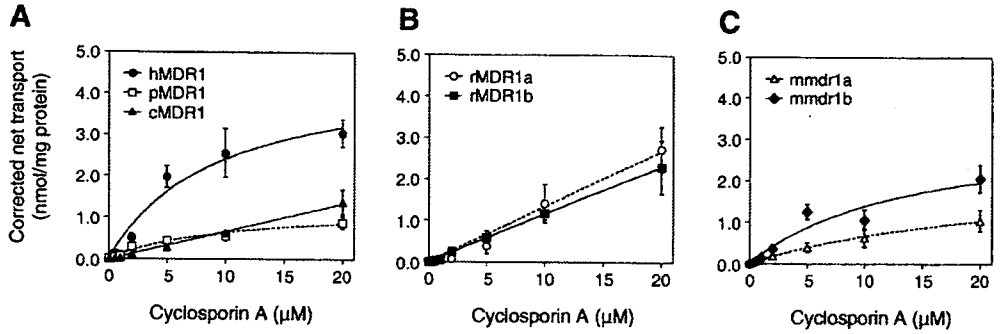

Figure 4. Net transport of cyclosporin A shown as the corrected V_{ad} value calculated by Western blot analysis using C219 antibodies across *MDR1* transfected cells: (A), hMDR1, pMDR1, and cMDR1; (B), rMDR1a and rMDR1b; (C) mmdr1a and mmdr1b. Each point represents the mean ± SEM of more than three determinations.

efflux ratio of rMDR1a were twice as high as those of rMDR1b.

Intracellular accumulations of cyclosporin A at 1 h of the B-to-A and A-to-B transports were increased with similar patterns in the P-gp expressing cells (data not shown). The intracellular accumulation from the B-to-A and A-to-B transport at 20 μM cyclosporin A ranged from 1.0 (rMDR1b) to 1.9 (rMDR1a) nmol/mg protein and from 0.6 (rMDR1b) to 1.7 (rMDR1a) nmol/mg protein, respectively.

Kinetic Analysis of Dexamethasone Transport

The transcellular transport of dexamethasone in *MDR1* transfected cells is shown in Figure 5. The corrected V_{ad} values estimated by the expression level of P-gp measured by Western blot analysis are shown in Figure 5A–C. The profiles of the V_{raw} and V_{ad} values were almost the same (data not shown). In all *MDR1* transfected cells except hMDR1, the V values were linear up to 1000 μM. Thus, we could calculate neither the V_{max} nor the V_{max}/K_m values of such cells. In comparison to the transport of diltiazem and cyclosporin A, pMDR1 and mmdr1a had a high capacity for dexamethasone transport.

The efflux ratio and corrected efflux ratio of dexamethasone transport at 37 nM are shown in Table 3. The efflux ratio and the corrected efflux ratio were similar except for mmdr1b.

Intracellular accumulations of dexamethasone from B-to-A and A-to-B transports at 1 h were increased with similar patterns in the P-gp expressing cells except rMDR1a and rMDR1b (data not shown). In the comparison between rMDR1a and rMDR1b, the B-to-A transport of rMDR1a was lower than that of rMDR1b, although the A-to-B transport of rMDR1a was higher than that of rMDR1b at 500 and 1000 μM dexamethasone.

DISCUSSION

Absorption, distribution, metabolism, and excretion are important factors in the pharmacokinetics

Table 2. Kinetic Parameters and Efflux Ratio of Cyclosporin A Transport across Monolayers of *MDR1* Transfected Cells

Cell Line	$K_{m,ad}$ (mL/mg/h)	V_{max} (nmol/mg/h)	$V_{max,ad}/K_{m,ad}$ (mL/mg/h)	$V_{max,ad}/K_{m,ad}$[a] (mL/mg/h)	Efflux Ratio	Corrected Efflux Ratio
hMDR1	9.3	4.6	0.50	0.50	19.1	7.0
pMDR1	10.0	2.0	0.20	0.13	25.1	9.2
cMDR1	>20	—	—	—	4.5	1.7
rMDR1a	>20	—	—	—	20.3	7.5
rMDR1b	>20	—	—	—	10.4	3.8
mmdr1a	>20	—	—	—	12.5	4.6
mmdr1b	14.1	3.8	0.27	0.24	15.9	5.9

[a]The corrected $V_{max,ad}/K_{m,ad}$ value calculated using the corrected $V_{max,ad}$ value, which was obtained by taking the relative expression level of P-gp measured by Western blot analysis using C219 antibodies into considerations.

The kinetic parameters were calculated as described in Materials and Methods. Efflux ratio was calculated at 66 nM cyclosporin A.

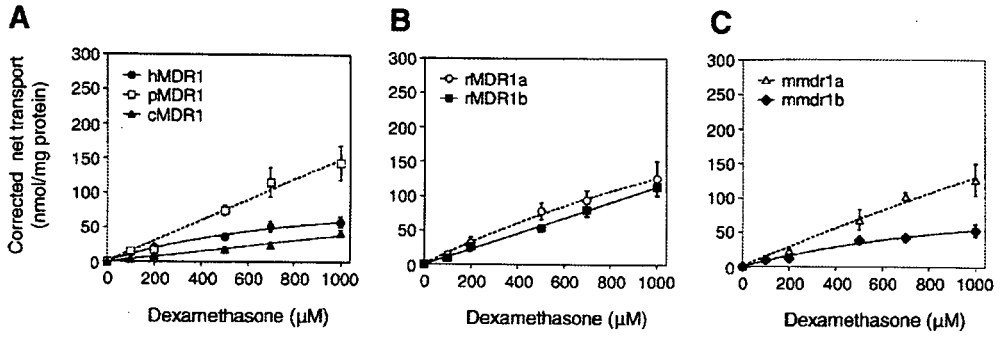

Figure 5. Net transport of dexamethasone shown as the corrected V_{ad} value calculated by Western blot analysis using C219 antibodies across *MDR1* transfected cells: (A), hMDR1, pMDR1, and cMDR1; (B), rMDR1a and rMDR1b; (C) mmdr1a and mmdr1b. Each point represents the mean ± SEM of more than three determinations.

of a drug and are influenced by the effects of ATP-binding cassette proteins such as P-gp. *In vitro* studies using *MDR1* transfected cells and *in vivo* studies using *mdr1* knockout mice are frequently performed for drug discovery and the assessment of drug interactions.[13,14] To estimate and extrapolate the pharmacokinetics and bioavailability of a drug in human, information about species differences is important. However, there is almost no information on species differences in transcellular transport via P-gp. Therefore, we studied the transcellular transport across monolayers of human, monkey, canine, rat, and mouse *MDR1* transfected cells and tried to evaluate the species differences. We selected diltiazem, cyclosporin A, and dexamethasone as typical P-gp substrates, which were investigated using a monolayer efflux, ATPase, and calcein-AM assays by Polli et al.[15]

Concerning the diltiazem transport, both the apparent $K_{m,raw}$ and $K_{m,ad}$ values of *MDR1* transfected cells showed 0.3–4.6-fold differences compared to hMDR1, suggesting that the affinity to diltiazem would differ among species. The apparent $K_{m,raw}$ and $V_{max,raw}$ values were almost the same as the $K_{m,ad}$ and $V_{max,ad}$ values, respectively, because there was almost no directed transport of diltiazem in mock cells. To estimate the P-gp-mediated transport, it is necessary to consider the non-transported permeability in an *in vitro* system. Although the apparent directed transport in mock cells was small, the kinetic parameters were estimated by the V_{ad} values in the present study. For the cyclosporin A transport, the apparent $K_{m,ad}$ values of cMDR1, rMDR1a, rMDR1b, and mmdr1a could not be obtained, because the concentration of cyclosporin A was set at below 20 μM due to the concentration of the organic solvent and cell toxicity. The apparent K_m value of the net transport of cyclosporin A in LLC-GA5-COL300 cells, in which human P-gp is overexpressed, was reported as 8.4 μM.[16] This was consistent with our result ($K_{m,ad}$ = 9.3 μM).

Table 3. Kinetic Parameters and Efflux Ratio of Dexamethasone Transport across Monolayers of *MDR1* Transfected Cells

Cell Line	$K_{m,ad}$ (μM)	$V_{max,ad}$ (nmol/mg/h)	Efflux Ratio	Corrected Efflux Ratio
hMDR1	896.1	248.6	7.0	5.0
pMDR1	>1000	—	9.3	6.7
cMDR1	>1000	—	9.2	6.7
rMDR1a	>1000	—	8.5	6.1
rMDR1b	>1000	—	15.6	11.2
mmdr1a	>1000	—	7.4	5.4
mmdr1b	>1000	—	15.9	7.1

The kinetic parameters were calculated as described in Materials and Methods. Efflux ratio was calculated at 37 nM dexamethasone.

Since the V_{max} value would depend on the P-gp expression level, we tried to quantify the P-gp expression level by Western blot analysis. It has not been quantitatively evaluated the reactivity of the C219 and H241 antibodies to each P-gp, although the P-gps of all species in this study could be detected. The recognized amino acid sequences of the H241 antibodies have not been clarified, but those of the C219 antibodies have been reported as VQEALD and VQAALD.[17] The VQEALD sequence was found in the same location of P-gp in all species of the present study, but that of VQAALD existed only in rat P-gp encoded by *MDR1a* and *MDR1b*, and mouse P-gp encoded by *mdr1a* and *mdr1b*. The corresponding sequences of human, monkey, and canine P-gps

DOI 10.1002/jps

were VQVALD. Therefore, the expression levels of P-gp measured by C219 antibodies could be compared among hMDR1, pMDR1, and cMDR1 or among rMDR1a, rMDR1b, mmdr1a, and mmdr1b. For the diltiazem transport, the corrected $V_{max,ad}/K_{m,ad}$ values of hMDR1 and pMDR1 were similar, but were different from that of cMDR1. The corrected $V_{max,ad}/K_{m,ad}$ values of rMDR1a and rMDR1b were significantly different. These differences may have been mainly caused by differences in the $K_{m,ad}$ value. However, for cyclosporin A transport, the $V_{max,ad}$ value affected the difference in the corrected $V_{max,ad}/K_{m,ad}$ values between hMDR1 and pMDR1, since their $K_{m,ad}$ values were similar. Differences in the $K_{m,ad}$ and $V_{max,ad}$ values among various P-gps would depend on the substrate.

The efflux ratio is frequently used to estimate whether a compound is a P-gp substrate or not. In the present study, the efflux ratio at a low substrate concentration was not correlated with the kinetic parameters. The efflux ratio and the corrected efflux ratio were different for cyclosporin A transport, although they were similar for diltiazem transport. Both the B-to-A and A-to-B permeabilities of cyclosporin A in mock cells were approximately 1/10 of the transport in *MDR1* transfected cells. The slight difference between the permeabilities in both directions in the mock cells had little effect on the net transport, but it had a certain effect on the corrected efflux ratio. The efflux ratio of cyclosporin A transport in cMDR1 showed a low value but the V_{ad} value was not extraordinary, as shown in Figure 4A. The reason for this phenomenon is still unclear. The efflux ratio is easy to calculate by measurement at one concentration of a compound. In addition, the corrected efflux ratio in *MDR1* transfected cells could be used to predict the penetration to the brain[5,8] and to evaluate the function of small intestinal P-gp.[18] However, it may be difficult to evaluate species differences with one concentration of a substrate. When species differences are estimated using the efflux ratios, it is reasonable to determine whether the efflux ratios of various substrates can be correlated between two species, as described by Takeuchi et al.[9]

The intracellular accumulation is another parameter of P-gp-mediated drug transport activity. The changes in the intracellular accumulation were not correlated with the transcellular transport and efflux ratio. All the parameters described above are practicable, but they may show disparate characteristics of P-gp. In the present study, we mainly focused on the kinetic parameters obtained from the net transport.

Chiou et al.[19] reported that the correlation of the oral absorption between human and canine for 43 drugs was relatively poor ($r^2 = 0.51$) and suggested that the apparent intestinal first-order absorption rate constant of drugs might be higher in canine than in human. In the present study, although the kinetic parameters in cMDR1 could be estimated only for the diltiazem transport, the $V_{max,ad}/K_{m,ad}$ value in cMDR1 was low. When the P-gp expression level was corrected by the Western blot analysis using C219 antibodies, the V_{ad} values of diltiazem, cyclosporin A, and dexamethasone in cMDR1 were lower at all concentrations than those in hMDR1. The difference in the absorption between canine and rat was due to differences in the pore size and frequency of pores in the paracellular pathway.[20] Although further study is needed to clarify the reason for the better absorption in canine, the lower activity of canine P-gp might be one of the important factors. Between human and monkey, there was a good correlation in the oral absorption for the 43 drugs.[21] As compared with the present study, there was a correspondence with the result of diltiazem but Chiou and Buehler[21] did not perform a comparison for cyclosporin A absorption. In the present study, the mouse P-gp encoded by *mdr1a* and *mdr1b* exhibited different profiles for diltiazem, cyclosporin A, and dexamethasone transport. This was not surprising because the two mouse P-gps have been reported to have the different properties for progesterone[22] and ramosetron transport.[23]

Molden et al.[24] suggested that there were species differences in the bioavailability of diltiazem. Species differences in the P-gp-mediated drug transport activity may be one of the reasons. Recently, Walker et al.[25] tried to elucidate the species differences in the disposition of UK-427857 and concluded that the transporter-mediated process would be a major factor in this phenomenon. To extrapolate data from animal to human, reliable information concerning species differences in P-gp-mediated drug transport activity would be useful.

In conclusion, species differences in P-gp-mediated transport become apparent when the kinetic parameters calculated by the net transport are used as an index. The species differences may depend on the substrate. It is controversial how the effect of P-gp *in vivo* on the absorption, distribution, and bioavailability can be estimated.